An Analysis of Trailing Suction Hopper Dredger Dredge Plume Development and the Use of Suspended Sediment Source Terms

A numerical simulation study

MSc Hydraulic Engineering
M.P.J. Willemsen

Delft University of Technology

TU Delft

An Analysis of Trailing Suction Hopper Dredger Dredge Plume Development and the Use of Suspended Sediment Source Terms

A numerical simulation study

by

M.P.J. Willemsen

October, 2022

Graduation committee	Prof. Dr. Ir. S.G.J. Aarninkhof
	Prof. Dr. Ir. W.S.J. Uijttewaal
	Dr. Ir. S.M.S. Alhaddad
	Dr. Ir. L. de Wit
	Ir. T. Van der Biezen

Institution: Delft University of Technology
Place: Faculty of Civil Engineering, Delft

TU Delft

Acknowledgement

Any piece of research is like a journey into new territory. This thesis took me to the turbulent world of dredge plumes. The waters were choppy and I met plenty of challenges along the way, but as the research proceeded, my interest in the subject deepened. Not only because it is a challenging topic, but also because of its environmental relevance.

I want to offer my profound and heartfelt gratitude to a number of people who encouraged and supported me while I was working on this project. Firstly, I thank the members of my graduation committee: Stefan Aarninkhof, Wim Uijttewaal, Said Alhaddad, Tim van der Biezen and Lynyrd de Wit. Their expert comments and knowledgeable insights were very valuable to me and the inspiring conversations I had with them kept me on track.

Second, I would like to thank the complete Hydronamic team, who welcomed me in their midst when I embarked on this project for Boskalis. On a regular basis, I engaged them in discussions about my project, and these contacts were always both enjoyable and useful.

And last but not least, I want to thank my parents Désirée and Hans, my siblings Rosalie, Esmeralda and Florian, my partner Jan and his family and my housemates Sanny and Koen. Without their continual and unwavering support, this project would have been much more cumbersome and less enjoyable.

Marguérite Willemsen
Delft, October 2022

Abstract

Dredging is performed for various reasons, including port development, coastal defense and land reclamation. The economic and social importance of such projects is widely acknowledged, but there are growing concerns about the possible environmental impact of the dredge plumes that form as a temporary by-product of these activities. Suspended sediment blocks sunlight, and sediment that settles on the seabed buries coral and other organisms. These effects accumulate over the duration of a dredging project, and should be minimized.

An important step towards this goal is predicting plume formation and development. Here, we focus on an overflow plume from a trailer suction hopper dredger (TSHD). Although this subject has been studied for years, much is still unknown, due to the complex interaction of the processes involved. Because of this complexity, it is not uncommon in the industry to use rules of thumb, derived from empirical studies.

One such rule of thumb, based on an influential publication by Becker et al. (2015), relates to the fraction of the overflow plume that is still (or again) in suspension once the developing plume moves from the dynamic near-field to the passive far-field. This source term fraction (STF) is important, because the large-scale area models that model plume development in the far-field require information about the characteristics of the plume entering the far-field zone. Becker et al. (2015) presented a realistic range of 0-20% for the source term fraction. This range is based on a combination of measurements and expert opinions. Although Becker et al. (2015) recommend characterization monitoring at the start of a dredging project to determine whether the 0-20% range needs adjusting, this is not always done in practice, due to time pressure, costs, complexity or lack of necessity.

Building on the work by Becker et al., this thesis aims to support a more informed implementation of TSHD source terms on the computational grid of far-field models. In order to explore the behavior of TSHD dredge plumes, numerical simulations were carried out using computational fluid dynamics model TUDflow3D. In these simulations, the values of three model input parameters – the water depth, the overflow density and the crossflow velocity – were varied to gain insight into the behavior of the plume under the conditions studied. For each of the three parameters, three representative values were chosen on the basis of expert advice, and all combinations were tested, leading to 27 numerical simulations.

The results of the numerical simulations show that the amount of sediment in the plume has reduced to less than 20% of the sediment in the overflow plume at 11-42 minutes of plume development, corresponding to a distance of 0-1895 m from the dredging location (500-3800 m from the moving vessel), depending on the specific conditions. It is important to note that (only) three conditions were varied in this study. These conditions were all steady state (e.g. no tidal flows). In real-life situations, many more (combinations of) conditions and hence a wider range of results are possible. Conditions where the plume was found to travel relatively long and far into the far-field, are a high ambient current, a low water depth and low overflow densities. The effect of these factors corresponds with existing studies.

The contribution of this work lies in the broad characterization of the developing plume under these various conditions: not only the magnitude of the plume is investigated, but also its vertical and lateral distribution. Specifically, the contribution of the bottom 6-13 % of the water column to the total plume flux is highlighted. This is particularly of interest, as this zone is typically not included in ADCP measurements. This increases insight in the processes underlying plume development and supports the appropriate determination and implementation of the far-field source term, including a more informed use of the 0-20% source term fraction range proposed by Becker et al. (2015).

Caution should be taken when implementing source terms in far-field models as a virtual source, as is common practice with the 20% source term fraction as presented by Becker et al. (2015). Implementing the 20 % source term fraction at the location of dredging activity leads to an underestimation of SSC and far-field fluxes. When implementing source terms, the user should also be advised that TSHD overflow plumes have a cross-sectionally skewed character for relatively long plume ages. It is advised to involve near-field modelling, field measurements and/or prior research (such as the results of this study) in order to make informed far-field modelling choices (e.g. the optimal vertical distribution of sediment).

Contents

Nomenclature

Abbreviations

Abbreviation	Definition
ADCP	Acoustic Doppler Current Profiler
BHD	Buckhoe Dredger
BLD	Bucket Ladder Dredger
CFD	Computational Fluid Dynamics
CSD	Cutter Suction Dredger
DNS	Direct Numerical Simulation
EIA	Environmental Impact Assessment
GB	Grab Dredger
JICF	Jet in Crossflow
LES	Large Eddy Simulation
OBS	Optical Backscatter Sensor
PICS	Particle Imaging Camera System
PSD	Particle Size Distribution
RANS	Reynolds Averaged Navier Stokes
SD	Suction Dredger
SDG	Sustainable Development Goal
SSC	Suspended Sediment Concentration
ST	Source Term
STF	Source Term Fraction
TSHD	Trailing Suction Hopper Dredger
VOF	Volume of Fluid
WALE	Wall Adapted Local Eddy viscosity
WID	Water Injection Dredger

Symbols

Symbol	Definition	Unit
u_{cf}	Crossflow velocity	[m/s]
w_0	Outflow velocity	[m/s]
Ri	Richardson number	[-]
g	gravitational acceleration	[m/s^2]
Re	Reynolds number	[-]
D	Initial jet diameter	[m]
d	Particle diameter	[m]
w_s	Settling velocity individual grain	[m/s]
Re_p	Particle Reynolds number	[-]
J	Vertical mass flux	[kg/s]
E	Resuspension rate	[kg/s]
D	Deposition rate	[kg/s]
Ri_l	Local plume Richardson number	[-]
D_l	Local plume width	[m]

Symbol	Definition	Unit
C_l	Centerline plume concentration	[kg/m^3]
U_l	Centerline plume velocity	[m/s]
C_0	Initial plume concentration	[kg/m^3]
D_0	Initial plume diamter	[m]
t	Time	[s]
u	Fluid velocity vector	[m/s]
P	Dynamic pressure	[kg/m^3]
C_l	Volume concentration for each fraction (Eq. 3.2)	[-]
D_p	Particle diameter (Eq. 3.5)	
$w_{0,f}$	Floc settling velocity	[m/s]
D_f	Floc diameter	[m]
Re_f	Floc Reynolds number	[-]
u_a	Ambient current velocity	[m/s]
u_{tshd}	Sailing speed	[m/s]
ρ	Density	[kg/m^3]
$\rho_{overflow}$	Overflow density	[kg/m^3]
Γ	Diffusion coefficient	[m^2/s]
ρ_0	Initial overflow density	[kg/m^3]
ρ_l	Density of individual fraction	[kg/m^3
ρ_a	Ambient water density	[kg/m^3]
ρ_p	Particle density	[kg/m^3]
ζ	Velocity ration	[-]
μ	Dynamic viscosity	[Ns/m^2]
ν	Kinematic viscosity	[m^2/s]
τ_b	Bottom shear stress	[N/m^2]
τ_d	Critical shear stress for deposition	[N/m^2]
τ_c	Critical shear stress for (re)suspension	[N/m^2]
ρ_l	Local centerline density plume	[kg/m^3]
τ	Viscous shear stress	[N/m^2]
ν_e	Eddy viscosity	[m^2/s]
ν_m	Molecular viscosity	[m^2/s]
ν_e	Turbulent viscosity	[m^2/s]

List of Figures

List of Tables

1

Introduction

Dredging operations are an integral part of hydraulic engineering operations; it is hard to imagine a world without them. For centuries, humans have carried out water infrastructure projects and manipulated the interface of land and water. This often involves dredging, which can be described as the underwater excavation of sediments and depositing them elsewhere. Dredging activities are executed to ensure the navigability of ports and waterways, to reclaim land and to protect our shorelines, amongst others. The industry's total turnover is sizeable, amounting to approximately 5 billion euros per year (IADC, 2020a). There are several reasons why this number can be expected to increase in the coming years. The first reason is demographic developments. The global population is rising, and a growing percentage of people is living close to a coastline. This will increase the need for goods and services, which can be expected to translate into an increase in waterborne transport (IADC, 2010). Other important reasons are the phenomena of sea-level rise and extreme weather conditions, both of which lead to a need for coastal protection projects. A third reason are offshore energy sources, such as wind energy, that require the construction of infrastructure (IADC, 2020a).

For dredging, various types of equipment can be used. The most appropriate choice of equipment for a specific dredging task depends on the characteristics of the equipment, the characteristics of the location and the demands of the job. The main types of equipment are hydraulic, mechanical/hydraulic, mechanical and hydrodynamic dredgers (Van Raalte & Parys, 2018).

- **Hydraulic dredgers** use centrifugal pumps to transport material sucked up from the bottom. the Suction Dredger (SD) is the simplest form of this type of dredger.
- **Mechanical/hydraulic dredgers** also make use of centrifugal pumps and can be divided into two types: the first is the Cutter Suction Dredger (CSD) that removes (harder) soils from the bottom with a rotating cutter, and the second is the Trailing Suction Hopper Dredger (TSHD).Transport of the material to the relocation site is carried by the ship itself. On arrival, the load is placed. The TSHD is often used for capital and maintenance work.
- **Mechanical dredgers** use mechanical excavation equipment. This category contains three types: the Grab Dredger (GD, a cable crane on a vessel), the Bucket Ladder Dredger (BLD, which uses a rotating chain with buckets for digging up and hauling up material) and the Backhoe Dredger (BHD, a hydraulic excavator on a pontoon).
- **Hydrodynamic dredgers** This type of dredging is less suitable for sensitive areas. An example of a hydrodynamic dredger is the Water Injection Dredger (WID, which injects water into the bed in order to enable it to be advected and to settle downstream).

This research will focus on the TSHD, one of the most commonly used vessels in the dredging industry. Approximately 600 of these vessels were active internationally in 2020 (IADC, 2020b). Moreover, the TSHD is one of the largest sources of turbidity caused by dredging.

1.1. Trailing suction hopper dredger

TSHDs are equipped with one or two suction pipes which are connected to a draghead which positions itself on the sea bed for operation. During operation, the suction pipe is let down from the vessel onto the sea bed. The draghead, equipped with water jet nozzles, allows the mixing of the sediment with water. A sand-water mixture is then pumped up through the suction pipe and subsequently deposited into the hopper of the vessel. Here, the sediment in the mixture starts settling under the influence of gravity. The excess process water then exits the hopper through a spillway called the overflow. Not all sediment will have had sufficient time to settle in the hopper. Part of the sediment that enters the hopper will leave with the overflow discharge. The sediment in the overflow discharge will be predominantly made up of fine grains, since coarse grains will settle faster in the hopper. The release of this overflow results in an a turbidity plume in the ambient water. The overflow plume is not the only sediment release mechanism of the TSHD.

Aside from this overflow plume, Becker et al. (2015) distinguish two secondary sources of sediment suspension by a TSHD: sediment released in the water column through draghead disturbance and (re)-suspension due to propeller wash, see Figure 1.1. The propeller wash also influences the overflow plume: the propellers increase suspended sediment concentrations by (re-)distributing sediment in the water column.

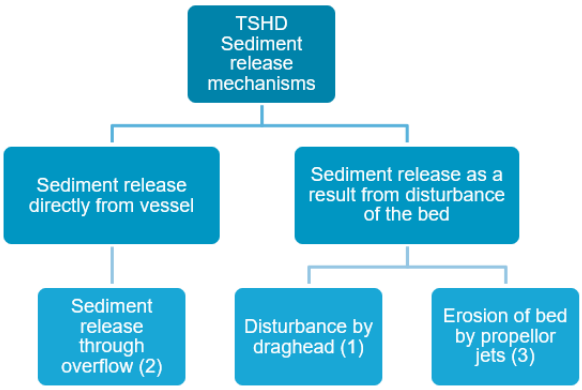

Figure 1.1: Sediment release mechanisms TSHD. Inspired by: (Becker et al., 2015)

Figure 1.2 shows a visual representation of the main suspended sediment sources for a TSHD. The numbers correspond to the numbers in Figure 1.1. When overflowing is allowed during the dredging operation, the overflow plume is the dominant source of suspended sediment (Decrop et al., 2018). Outside of the immediate vicinity of the dredger, the combined dredge plume, consisting of all three plume sources, will be taken along by the ambient currents and will eventually settle.

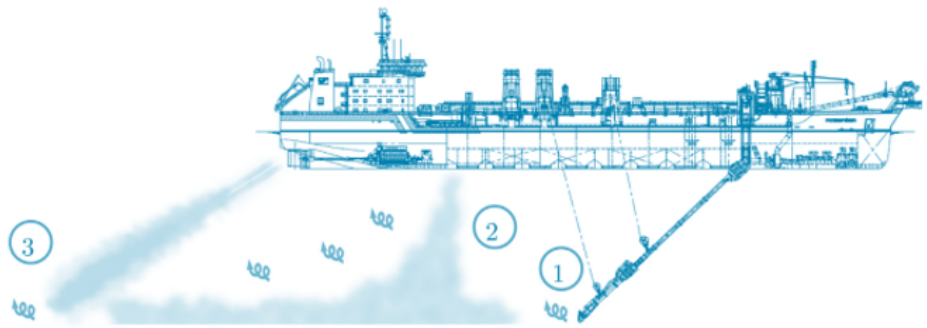

Figure 1.2: Visual representation of different plume sources of a TSHD. The numbers (1) (2) and (3), correspond to the numbered plume sources in Figure 1.1. Adapted from: (Becker et al., 2015)

1.2. Environmental impact of dredging

The past few decades have shown an increasing interest in the environmental aspects of dredging. The well-known and impactful report Our Common Future, commissioned by the General Assembly of the United Nations in the 1980s, introduced the concept of sustainable development. The report pointed at the interdependencies between economic, social and environmental developments, urging all nations to take a holistic view of where we are going (World Commission on Environment and Development, 1987). Since the report was published, the concept of sustainable development gradually took root in society. The next big milestone in focusing the worlds attention to this subject was the introduction of the Sustainable Development Goals (SDGs) by the United Nations in 2015 (United Nations, 2015).

Dredging is related to many of the 17 SDGs, for example to the goal of building resilient infrastructure, and contributing to these goals is an opportunity for the sector in the years to come (Bridges & Vellinga, 2018). The dredging industry is aware of the need for sustainable development, and increasingly strives for a harmonious integration of the socioeconomic and environmental aspects of dredging projects. Many contractors perform environmental assessments in the proposal phase on their own account in order to identify potential environmental impacts and positively differentiate themselves from competitors. Taking environmental considerations into account is also a necessity, because of increasing legislative pressure (Vikolainen et al., 2014). Various stakeholders also increasingly emphasize sustainability (Wasim & Nine, 2017).

1.2.1. Noise, emissions and contaminants

Four main sources of environmental impact are increased sound levels, emissions, released contaminants and increased suspended sediment concentration (SSC) (Adnitt & Van Koningsveld, 2018). With regard to dredging sounds, a review of studies by Wenger et al. (2017) showed that these sounds can affect fish in several ways (behavioral changes, temporary hearing loss, stress). The precise effects depend both on the type of fish and the sound pressure of the dredging project. The authors point out that much is still unknown and more research is needed. Another source of environmental impact comes from emissions. Dredging vessels emit greenhouse gases and other harmful emissions, such as SOx and NOx (Castro et al., 2019). These emissions have a range of adverse effects, which are considered well-known. The next source of impact discussed here are contaminants. These polluting or poisonous substances typically adhere to fine sediment, and can end up in the water during dredging activities. The earlier mentioned review by Wenger et al. (2017) shows that the impact of contaminants on fish is greater than that of dredging sounds or suspended sediment. The effects include behavioral, physical and/or physiological impacts and a number of studies also report mortality.

1.2.2. Turbidity

The last source of environmental impact discussed here, and the one most relevant for this study, is the suspended sediment concentration (SSC). SSC indicates turbidity, the cloudiness of the water. In cloudy water, the rays of the sun penetrate less deeply. There can also be more sedimentation. These factors can affect aquatic ecosystems. Flora or fauna in the area of influence of the project that might be affected by the proposed activity are called sensitive receivers (Adnitt & Van Koningsveld, 2018). It should be noted that such receivers might also be exposed to turbidity from sources other than dredging; ecosystems can exist in areas with naturally high turbidity.

Erftemeijer et al. (2012) studied existing literature on the sensitivity of corals to turbidity and sedimentation, especially when caused by dredging. The authors concluded that the sensitivity of coral reefs to a high SSC depends on many factors and varies significantly; the most sensitive corals survive no more than a few days of high turbidity. Sedimentation is a stressor as well; amongst others, it can cause smothering and shading. Also with respect to these stressors, the sensitivity of corals varies strongly. Some species cannot survive 24 hours when the sedimentation rate is high. Coral larvae, too, suffer from turbidity and sedimentation (Erftemeijer et al., 2012).

Research by Cunning et al. (2019) shows the considerable impact that dredging can have on the environment. The study relates to dredging activities that took place between 2013 and 2016 to make the Port of Miami shipping channel wider and deeper. The total amount of dredged material was 4.2 million m^3. The presence of dredging plumes was established by means of remote sensing. Sediment accumulation was measured with sediment traps; coral condition and habitat were determined through observations. The results show that the dredging plumes extended from 10 km south of the dredged area to 15 km north, and that the impact of the plumes was both long-lasting and widespread. Using data-driven methods, the authors found a high correlation between the presence of dredging plumes, sediment trap accumulation, and (partial) burial of coral. The probability of partial or complete burial of coral rose sharply after dredging commenced, and parts of the benthos were still covered deep in sediment after 2 years. The density of corals especially small corals - showed a significant decrease over this period. The authors estimate that over half a million were killed.

Marine mammals are generally used to turbid water, but they can be affected indirectly, because suspended sediment, turbidity and other dredging-related effects can impact communities of the organisms they prey on (Todd et al., 2014). Wenger et al. (2017) have found that suspended sediments have various adverse effects on fish, such as avoidance of the area, behavioral changes, and effects on foraging and predation.

1.2.3. Environmental impact assessment (EIA)

When sensitive receivers are identified in the project area, their ecological thresholds with respect to turbidity need to be determined. In order to then assess the potential impact of a TSHD dredge plume, a reliable prediction of the increased turbidity in the area of interest is required. Quantifying the increase in turbidity from dredge plumes is a crucial part of any Environmental Impact Assessment (EIA), both for regulatory approval and monitoring design purposes (Sun et al., 2020). Figure 1.3 depicts an overview of the processes that lead to a potential sensitive receiver response. As Figure 1.3 shows, quantifying the potential receiver response requires an ecological assessment and a turbidity assessment. This study focuses on the latter.

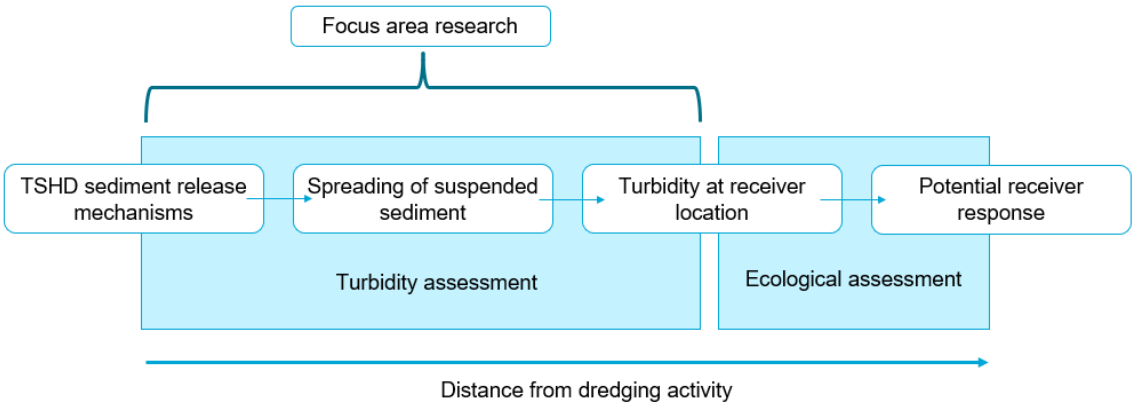

Figure 1.3: Flow chart depicting an overview of the required assessments to quantify potential receiver response to increased turbidity

The aim of a turbidity assessment is to quantify the amount of suspended sediment (SSC in mg/L) at the location of (potential) sensitive receivers. It should be noted that for such an assessment it is important to make a distinction between dredging-induced pressure on the ecosystem and the presence of natural sources of SSC as pointed out by Sun et al. (2020). Aarninkhof et al. (2008) also stress that turbidity can be induced by natural processes and/or other (human) activities.

1.3. Problem description

Conducting turbidity assessments is challenging through all phases of a dredging project. SSC predictions are inherently accompanied by uncertainty for a multitude of reasons. The exact metocean and soil conditions that will be encountered during the proposed works are not known. Also, details of the dredging operations are often not yet known, making it more difficult to accurately predict SSCs. Even when all above-mentioned details are known, predicting the development of a turbulent overflow plume is a challenge due to the complex mix of processes that is governing plume development.

1.3.1. Dynamic and passive plume

In the literature, distinctions are made between different 'zones' of the dredge plume. The most common classification, and the one that will be used for this study, is the distinction between a dynamic near-field and a passive far-field (e.g. by Laboyrie et al. (2018) and Sun et al. (2020)). A visual representation is shown in Figure 1.4.

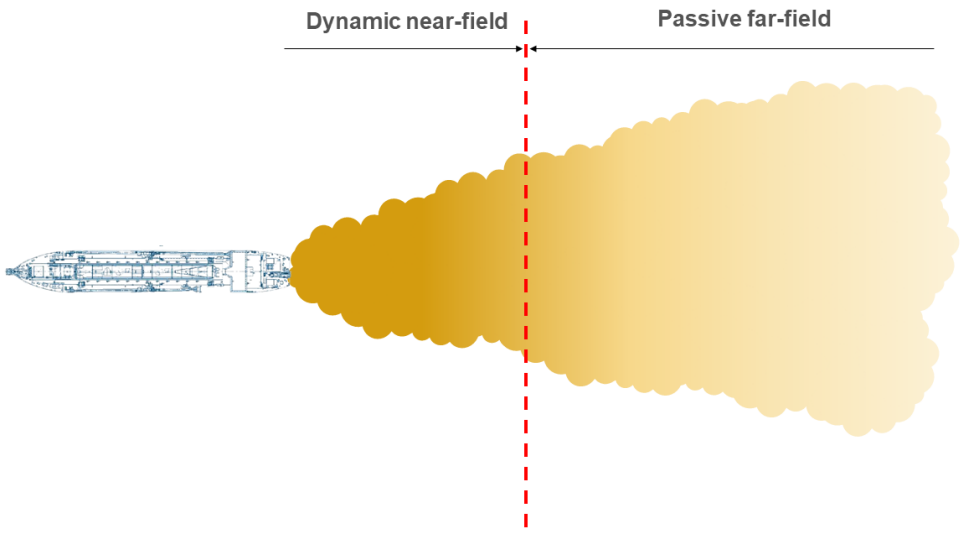

Figure 1.4: Top view TSHD induced dredge plume showing the common distinction between a dynamic near-field and a passive far-field

Although the exact definitions vary in the literature, there appears to be a general consensus with regard to the governing processes in the near- and far-field. These governing processes for each zone as described by De Wit et al. (2020) are summarized in Table 1.1. An in-depth review of these processes will be performed in Chapter 2.

Dynamic phase	Passive phase
Density driven behaviour	Ambient hydrodynamics
Entrainment of ambient water	Settling dynamics
Interaction with the vessel	

Table 1.1: Common classification between the dynamic near-field and the passive far-field based on the governing processes, as described by De Wit et al. (2020)

Although metrics can be defined to indicate the plume age or distance where the plume is no longer dynamic, such metrics are always somewhat arbitrary. In reality, no clear-cut location of a transition between a dynamic near-field and a passive far-field exists: the plume gradually becomes less dynamic with distance from the vessel until it is solely governed by the ambient hydrodynamics and can be classified as a passive plume. However, it is an important distinction from a modelling standpoint. It is essential to know which processes are governing plume development to make the best modelling choice:

1.3.2. Dredge plume modelling

Due to the substantial difference between the processes dominating plume behaviour in the dynamic and passive phase, the zones are typically modelled separately. In the dredging industry, the models that are used for modelling the passive phase are called *far-field models*. Depending on model choices (e.g. grid size), a far-field model will be able to capture some dynamic behavior. Therefore, it can be argued that the start of 'far-field' is also modelling choice.

Far-field modelling

The processes in the passive far-field occur on relatively large spatial and temporal scales. Therefore, well-known large-scale area models such as Delft3D and MIKE are well-equipped to simulate the pas-

sive sediment transport in the far-field (De Wit et al., 2020). Large-scale area models such as Delft3D simulate hydrodynamics by solving the 2D or 3D non-linear shallow water equations. The system of equations consists of horizontal momentum equations and the continuity equation. Delft3D works under the assumption of hydrostatic pressure. To simulate the transport of suspended sediment, Delft3D solves an advection-diffusion equation. The model requires boundary conditions, initial conditions and bathymetry to solve the system of equations. It should be noted that even though these large-scale area models are considered well developed, far-field modelling requires careful and informed choices regarding the number of dimensions used, grid sizes, diffusion coefficients, amongst others. Tuinhof (2014) made recommendations with regard to effective far-field modelling techniques. In general, the author concluded that a horizontally and vertically fine-grid 3D model leads to the most accurate results, but that less computationally expensive techniques may be warranted depending on the requested output.

Large-scale area models such as Delft3D generally have insufficient grid resolution to accurately represent the governing processes in the dynamic phase. As a result, these models demand the amount of suspended sediment entering the far-field as input. This is commonly called the far-field source term (Becker et al., 2015).

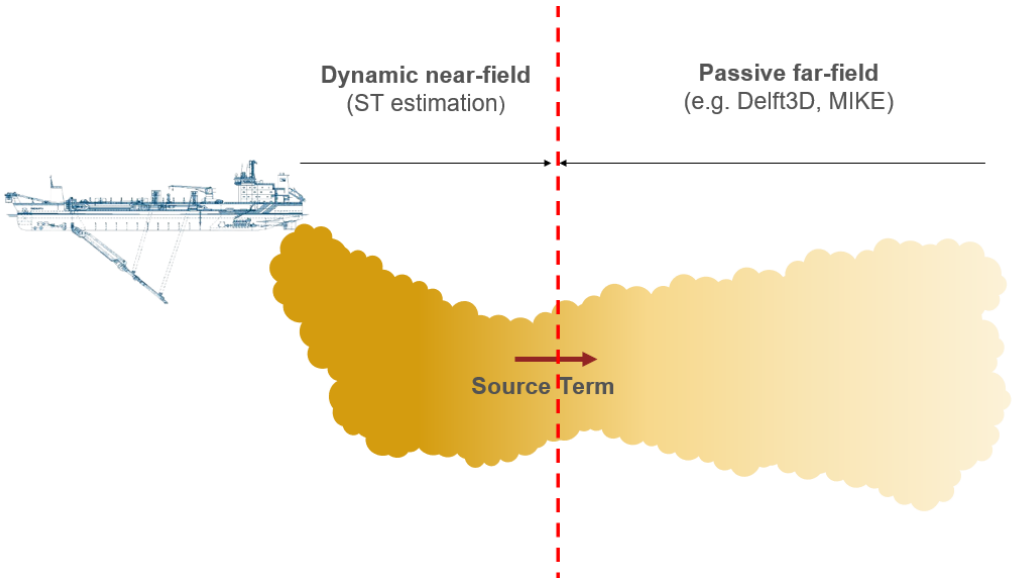

Figure 1.5: Representation of area of applicability far-field model and implementation location source term. Inspired by: Becker et al. (2015)

Souce term estimation

Reliable source term estimation is key to any assessment. The amount of sediment entering the far-field, the source term, can vary significantly depending on the type of dredging operation, the equipment, the bathymetry, site characteristics, etc (Sun et al., 2020). In the literature, it is generally agreed that estimating source terms is not an easy task. Sun et al. (2020) reviewed a sample of EIA documents and concluded that there is a lack of consistency and clarity surrounding the best approach to estimate source terms.

Measurement-based source term estimates may be used as a guide for preliminary inputs for passive plume modelling, provided that the proposed operations occur under similar conditions to those encountered during the measurements. Considering the magnitude of the range of possible combinations of conditions, work methods, materials and bathymetry, this method is not often applicable. Sun et al. (2020) also note that the number of field measurement campaigns of sufficient scope and quality to make reliable source term estimates, is limited. Another approach that is used in practice to make an (initial) estimate of the far-field source term is the source term fraction concept, a generic method presented by Becker et al. (2015).

The source term fraction concept as presented by Becker et al. (2015) is a generic approach which circumvents the modelling of near-field processes. It can serve as a complementary method to near-field modelling, which is computationally expensive. The method is also commonly used by the dredging industry for their initial estimate of the source term magnitude. In principle, the method tracks the fate of fines available in dredged material across different stages of the dredging operations. The method uses so-called source term fractions (STF) to relate the different contributions to the far-field source term to the total amount of fines available (Becker et al., 2015). The general approach of the method involves 4 steps, which are visualized in Figure 1.6.

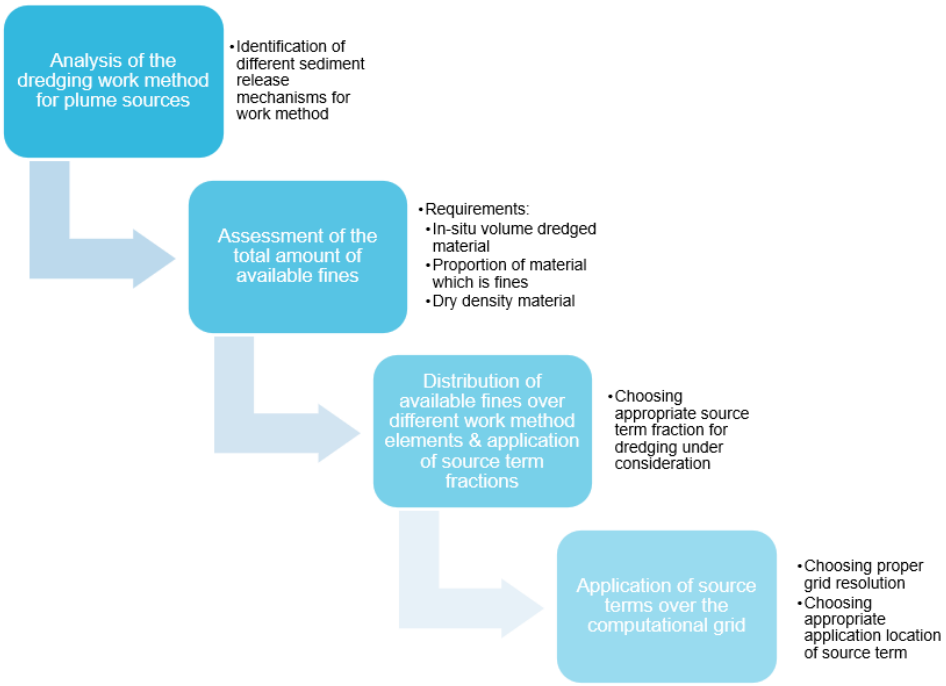

Figure 1.6: Visualization of the four steps of the Becker method required for source term estimation

An important step in the method is the third step, choosing appropriate values for the source term fractions. Regarding the empirical source term fractions required for step (3) the authors present reasonable ranges for a number of plume sources, which were derived based on a combination of practical experience and field monitoring campaigns (Becker et al., 2015). For the overflow source term fraction, a reasonable range of $0 - 20$ % is presented. Becker et al. (2015) emphasize that the application of the source term fraction concept introduces inherent uncertainties and that depending on the level of detail required, near-field modelling and/or monitoring is warranted. Aside from the authors' instruction to use these ranges with caution, a follow-up publication notes that measurements have shown that under certain circumstances, the overflow source term fraction can exceed 50 % (van Eekelen et al., 2015). This occurs when the water is shallow and the underkeel clearance is limited. in such cases, there can be a combined effect of the overflow plume and the propeller wash, leading to effective values of the source term fraction of over 50%. A more detailed understanding of the area of applicability of the reasonable range presented for the overflow source term fraction will allow for more reliable (initial) estimates of the source term.

Model coupling

The appropriate application of source terms on the computational grid of a far-field model, as prescribed in step (4) of the source term fraction concept, is easier said than done. Far-field modelling requires choices with regard to the number of dimensions, grid sizes, time steps etc. Tuinhof (2014) already

showed that these decisions should be informed and that the choices in this phase can greatly affect the outcome of the predicted concentration and/or flux that is found in the far-field. The intended input location of the source term on the far-field computational grid is at the transition between the near-field and far-field. When this transition falls within the size of a single grid cell, the cell where the dredging activity occurs is the appropriate input location. Partly due to the fact that a robust method for the determination of the location of the transition is lacking, source terms are often implemented at the location where the dredging activity occurs. Under circumstances where the spatial extent of the near-field spans multiple grid cells, this practical use of the source term is not in line with the intended use and estimates become less accurate. When a STF of 20% is implemented at zero meters from the dredging activity, whilst this STF in reality is found at a distance of 1 km, the resulting SSC at a distance of, for instance, 10 km will be underestimated. This is visualized in Figure 1.7. Implementing source terms in a far-field model also requires choices to be made regarding the vertical distribution of the source term (when using a 3D model). With more information on the magnitude of the plume (e.g. where do we find 20%?) and its vertical and horizontal distribution, the implementation of source terms can be more informed.

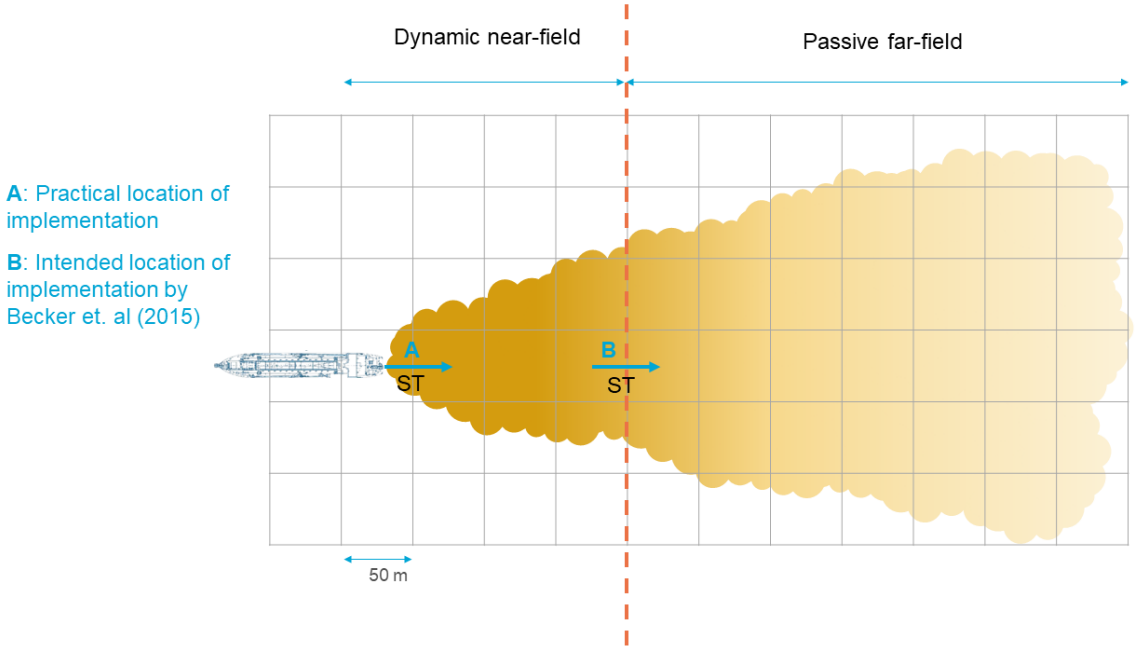

Figure 1.7: Schematization of a far-field computational grid and the (potential) difference between the intended location of implementation of a source term (ST) and the common practical location of implementation

1.4. Research objective

Far-field models require a source term as input representing the amount of sediment entering the far-field. In order to arrive at realistic predictions of SSC in the far-field, assumptions have to be made regarding:

1. The magnitude of the source term
2. The vertical and/or lateral distribution of the source term
3. The location of implementation on the far-field computational grid

As mentioned in Section 1.3.2, Becker et al. (2015) have presented the 'source term fraction concept': a guide for determining source term magnitudes (1) in the early phases of a proposal. The authors present reasonable ranges, based on measurements and practical experience, for the source term fraction: the amount of fines that are entering the far-field (as a % of the fines leaving the overflow). Focusing on

the TSHD, a reasonable range of 0-20 % is presented. The authors do not elaborate on aspects (2) and (3) mentioned above, but Tuinhof (2014) has shown the relevance of these aspects for achieving appropriate far-field predictions.

From this problem description, the following research objective has been formulated:

"The research aims to support a more informed implementation of TSHD source terms on the far-field computational grid"

This research objective translates into the following research questions:

1. At which plume age and distance from the dredging location is the 0-20% range for the overflow source term fraction, as introduced by Becker et al. (2015), found under various conditions?
2. Under various conditions, what is the character of the vertical and lateral distribution of the TSHD dredge plume?
3. How can current practice regarding the implementation of source terms be improved?

1.5. Methodology

A literature study is performed in order to gain insight into the governing processes of dredge plume development. The second research question aims to investigate the influence of various processes and characteristics on the magnitude of the source term. This is done by performing a numerical simulation study with TUDflow3D. Developed by De Wit (2015), TUDflow3D is a fully 3D Computational Fluid Dynamics (CFD) solver which makes use of the Large Eddy Simulation (LES) approach to capture the influence of turbulence in the near-field. TUDflow3d is a trusted and well-calibrated tool for the prediction of the fate and development of TSHD dredge plumes in the dynamic near-field.

1.5.1. Plume development

A set of scenarios will be designed by varying parameters in TUDflow3D within realistic ranges in different combinations. Model parameters are based on the base case of the dissertation of De Wit (2015) and are considered best practice. The scope of the scenario study is limited to varying ambient parameters (ambient water depth, ambient current velocity) and plume parameters (overflow density). The vessel's characteristics are kept constant. Since the spatial extent of the near-field varies, the choice is made to extend the TUDflow3D runs to 60 minutes of plume development, thereby including (part of) the far-field. The numerical simulation set-up is described in more detail in Chapter 3.

The resulting model output of the individual model runs are evaluated in terms of dredge plume character and magnitude. The magnitude is evaluated during various stages of plume development. Subsequently, the resulting source term magnitudes at various plume ages are compared to the reasonable range as presented by Becker et al. (2015). This gives insight into the relationship between the prevailing conditions and the area of applicability of the source term fraction concept.

1.5.2. Far-field implementation

The results from the detailed TUDflow3D simulations will be used to assess the current practice regarding the implementation of source terms on the far-field computational grid and gain insight into the potential inaccuracy of the current practice.

1.6. Structure of report

Chapter 2 starts with the relevant background theory on the development of overflow plumes and concludes with a review of the relevant studies on the topic. In Chapter 3, the methodology, TUDflow3D and its governing equations are introduced followed by the set-up of the numerical simulation study. In Chapter 4, the results are presented and interpreted. This report concludes with the discussion in Chapter 5 and conclusions and recommendations in Chapter 6.

2

Theoretical framework

This chapter starts with Section 2.1, Background Theory, which discusses the main processes that play a role in the formation and development of TSHD overflow dredge plumes. Knowledge about these processes helps interpret the behavior of plumes as predicted by TUDflow3D. In Section 2.2 a critical review is conducted of relevant literature.

2.1. Background theory

A substantial body of research exists on understanding the characteristics of discharges in marine environments. Wang and Mohammadian (2022) studied the impact of improperly discharged brine by desalination plants, focusing on the mixing of an inclined dense jet on a sloping bottom. The thermal-saline effluent of power plants has also been a popular topic of research. Both Ardalan and Vafaei (2019) and Zhao et al. (2018) conducted an experimental study focusing on the mixing characteristics of the thermal discharge of power plants. In the literature, most of these effluents are classified as turbulent buoyant jets, given that these effluents are discharges with both momentum and buoyancy. For the thermal discharge, the buoyancy is the result of a temperature and salinity difference whereas the buoyancy of an overflow discharge is caused by the increased density of the sediment-laden water (Taherian & Mohammadian, 2021).

An overflow jet can be classified as a special type of turbulent buoyant jet. Since the ejected sediment-water mixture is typically entering a non-stationary oceanic environment, it can be classified as a buoyant jet in cross-flow (JICF). Figure 2.1 shows the character of a typical buoyant JICF.

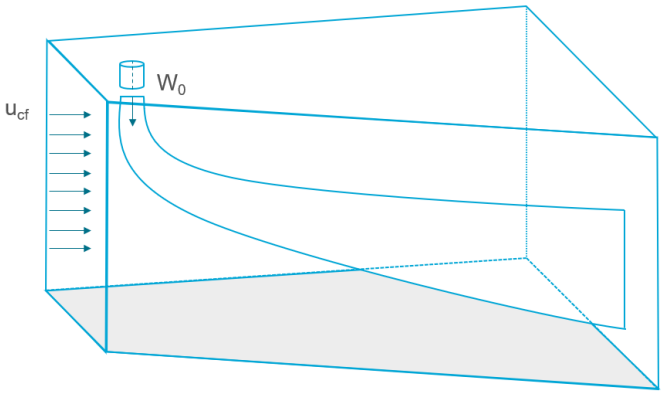

Figure 2.1: Characteristic Negatively Buoyant Jet in Crossflow

The jet, with an outflow velocity W_0, will interact with the crossflow, with a velocity u_{cf}, resulting in a complex pattern of three-dimensional non-linear flows (Dai et al., 2016). Cintolesi et al. (2019) distinguish three zones in a buoyant JICF: (a) the momentum phase, where the plume is mainly driven by the initial momentum, (b) the buoyancy phase, where the buoyancy force strongly pushes the plume upward/downward and (c) the entrainment phase where the cross-flow deviates the plume in horizontal direction. In these names, the dominant processes in the respective zones can be recognized. In combination, they lead to the typical shape of a dredge plume, depicted in Figure 1.5.

According to Tohidi and Kaye (2016), the bent-over behavior of a plume in crossflow is omnipresent in environmental fluid mechanics. The precise trajectory of the plume will depend on factors such as the degree of buoyancy of the jet, the initial momentum, the horizontal cross-flow momentum and the intensity of turbulence (De Wit, 2015).

As mentioned in Chapter 1, the governing processes vary with distance from the vessel, and we follow the distinction made in the literature between a dynamic near-field and a passive far-field. Section 2.1.1 relates to the dynamic near-field, where the dredge plume originates as a buoyant JICF. Section 2.1.2 discusses the passive far-field, where the plume disperses and is taken along by the ambient current.

2.1.1. Dynamic phase

According to Miedema and Becker (1993), dredge plumes are complex systems in which the physical processes play an important part. In this section, an overview is given of the processes governing the extent, intensity and development of an overflow plume in the dynamic near-field.

Descending and mixing
During TSHD dredging operations, sediment-laden process water is ejected from the vessel through the overflow shaft. This discharge can have sizeable initial momentum and is denser than the ambient water. This is called the dynamic phase (Spearman et al, 2007). During this phase, the plume may descend quickly to the seafloor under the influence of initial momentum and density differences. During its descent, the plume may entrain seawater and lose coarse particles. This leads to loss of momentum and density, and leads to mixing with the surrounding seawater. Mixing takes place before and after the plume has reached the seafloor. Once the plume has reached the seafloor, it will spread laterally as a density current. Ultimately, the plume becomes passive and is advected out of the near-field (e.g. De Wit, 2015, Van Eekelen, 2007). According to several authors (e.g. Winterwerp, 2002, Kemps and Masini, 2017), particle settling velocities are much less important in the dynamic phase than the bulk behavior of the plume. Following Fischer et al. (1979), Winterwerp (2002) notes that two dimensionless numbers govern the plume's behavior: the Richardson number Ri and the velocity ratio ζ. This is the ratio of the velocity of the ambient water relative to the vessel over the initial jet velocity. The author categorized overflow plumes in three different regimes based on these two numbers: a density driven regime, a mixing regime, and a transitional regime in between the two. Figure 2.2 shows this classification.

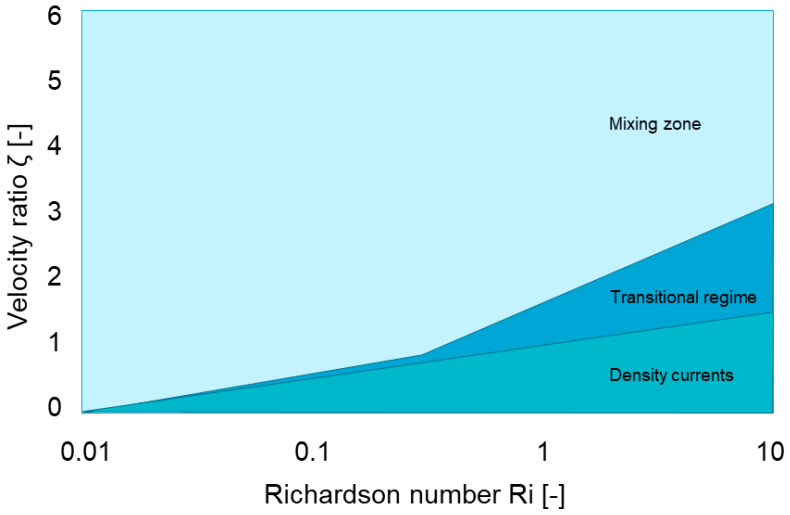

Figure 2.2: Different regimes overflow plume. Inspired by Winterwerp (2002)

The Richardson number can be seen as an indicator of the importance of buoyancy. A large Richardson number corresponds to a regime where buoyancy is dominant over kinetic energy (Sun et al., 2020). In such a regime, turbulent mixing is suppressed. Equation 2.1 shows that this is the case for large density differences between the water-sediment mixture and the surrounding water, a large diameter of the overflow, and low outflow velocities.

$$Ri = \frac{g\Delta\rho_0/\rho_{\mathrm{a}}\mathrm{D}}{W_0^2} \tag{2.1}$$

where:

g = gravitational acceleration
$\Delta\rho_0$ = difference in initial jet density and ambient water density
ρ_{a} = ambient water density
D = initial jet diameter
W_0 = initial outflow velocity jet

The velocity ratio, which is defined in Equation 2.2, represents the ratio between the ambient velocity and the initial jet velocity.

$$\zeta = \frac{u_{cf}}{W_0} \tag{2.2}$$

Revisiting Figure 2.2, it can be seen that the density driven regime corresponds to large Richardson numbers (buoyancy is dominant) and low velocity ratios. Under these conditions, the plume has a highly dynamic character.

A dense plume with an initial large diameter, a large velocity and a low ambient current, finds itself in the density-driven regime. A low density plume, on the other hand, with a small velocity in a fast ambient current, will be in the mixing regime. In the mixing regime there will be a higher availability of fine sediment for the passive plume and hence a higher source term fraction. It can be concluded that depending on the plume characteristics and ambient surroundings the plume will descend rapidly towards the bed or will be more prone to mixing in the immediate near-field.

According to Chen et al. (2022), common values for TSHD dredge plumes lie within the range of 0.3-4 for ζ and 0.1-10 for Ri. Looking at Figure 2.1, it is noteworthy that the velocity ratio plays a much larger role than the Richardson number in creating a density driven regime. Such a regime is possible at practically any realistic Richardson number, but the velocity ratio must be lower than 1.5.

Upward mixing
Under certain circumstances (high ζ, low Ri), a surface plume may arise in the near-field (Chen et al., 2022). Research by De Wit (2015) showed that a surface plume varies between 0-2% of the overflow flux (at normal dredging speed). As the name suggests, a surface plume consists of sediment that is not directly descending towards the bed, but initially mixes upward to the surface, creating a visible plume. A surface plume is visualized in Figure 2.3.

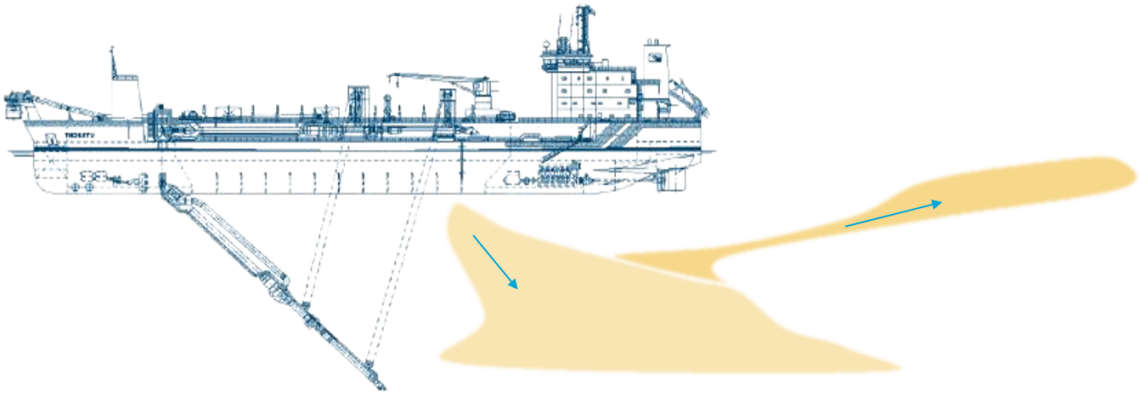

Figure 2.3: Surface plume generation

The existence and size of a surface plume affects the far-field source term, as the sediment can stay suspended for long periods and distances. De Wit et al. (2020) performed a range of CFD simulations and drew conclusions regarding the generation of a surface plume. The authors conclude that a large crossflow velocity, this is the sum of the ambient current and dredging speed, results in the generation of a surface plume. This is confirmed by Decrop and Sas (2018), who also performed CFD plume simulations. Other factors resulting in the generation of a surface plume are limited dredging depth and air entrainment.

As the name suggests, air entrainment refers to the presence of air bubbles in the overflow shaft. Due to the positive buoyancy of the entrained air bubbles, the sediment plume will settle more slowly (Saremi, 2014). The reason is that escaping air bubbles drag some of the smaller sediment particles along. Therefore, air entrainment results in a longer-lasting dredge plume. The phenomenon can be combatted by the use of an environmental valve / a green valve. These measures reduce the flow of air that is trapped in the overflow. As a result, the dynamic plume descends more quickly to the seabed, effectively reducing the turbidity.

Influence of external factors
Operational dredging factors such as the dredging speed, propellers, overflow location and pulsing frequency also play a role. Pulsing refers to a discontinuous flow due to ship movements. Using Large Eddy Simulation (LES), De Wit et al. (2014) studied the effect of these external factors on the mixing of plumes in the near-field and on the formation of surface plumes. It was shown that a higher dredging speed leads to less dilution of the plume; the plume stays closer to the surface and there is less mixing. The authors also found that pulsing leads to a larger vertical spread of the sediment. Factors that contribute to the formation of a surface plume are a high dredging speed, a propeller and pulsing. These factors all lead to the stripping off of sediment particles from main plume, thus contributing to the surface plume. It was also shown that an overflow location at the back leads to a larger surface plume at normal speed.

Another external factor is the water depth. Winterwerp (2002) hypothesized that in transitional regimes (which combine density-currents with mixing) a very large water depth gives ambient currents more

time to mix with the plume and/or strip particles off the plume, leading to more dilution before the plume hits the bed. De Wit et al. (2020) found that a shallow water depth is an important factor for the creation of a surface plume.

2.1.2. Passive far-field

Gradually, the dynamic near-field transitions into the passive far-field. Following Sun et al. (2020), the far-field is described here as the zone where the dynamic plume has weakened and is being spread by the ambient hydrodynamics and the settling of the suspended sediment under the influence of gravity. According to (Spearman et al. (2007), sediment particles can end up in the passive plume in various ways: as a result of separation from the rapidly descending dynamic plume, as a result of impacting the near-field bed, or after travelling along the bed as part of the bed plume. Kemps and Masini (2017) point out that, because the plume has already partly dispersed in the near-field, and the coarser particles have settled there, the suspended sediment concentration is low by the time the plume arrives in the far-field. It typically consists of fine material such as silt and clay. Differences in density and momentum have become minimal, and transport in the far-field takes place by ambient hydrodynamics, settling velocities and deposition and/or resuspension at the seafloor. These processes will now be briefly discussed.

Dispersal by ambient hydrodynamics
According to Spearman et al., (2007), the passive plume mixes with the ambient water, and slowly disperses as a result. According to the authors, two mechanisms govern this process: turbulent diffusion and shear dispersion. A third mechanism is also responsible for mixing; molecular diffusion, but this is negligible on large scales for high Reynolds numbers flows, which we are dealing with. Shear dispersion, which is dominant over turbulent diffusion, refers to particles having different directions and speeds at different heights as a result of the current velocities in the water column. This will lead to dispersion of the plume.

Settling dynamics
Settling dynamics play an important role in dredge plume development, especially in the far-field. Sediment settling of individual grains is generally well-understood. However, the occurrence and relevance of aggregation processes such as flocculation in dredging plumes is poorly understood.

Smith and Friedrichs (2011) explain that particle settling is the combined effect of three forces: gravity, buoyancy and drag. These forces are influenced by properties of the fluid (density, viscosity) and the particles (density, shape, size, permeability). The particle settling velocity is commonly described by Stokes Law which is described in Equation 2.3.

$$w_s = \frac{(\rho_p - \rho_a)\, g d^2}{18\mu} \tag{2.3}$$

where:

w_s = settling velocity
ρ_p = density of the particles
d = diameter of particles
μ = dynamic viscosity

Small particles Reynolds numbers ($\mathrm{Re}_p = w_s d/v \ll 1$ where v is the kinematic viscosity) and impermeable, spherical particles are assumed when applying this law. From Stokes Law it is clear that aggregation processes will influence sediment settling. Smith and Friedrichs (2011) explain that aggregate particles can have various origins. Some have aggregated in the bed before being dredged up, while others have aggregated in the water column as a result of flocculation. Flocculation also takes place in the TSHD. Regardless of how they ended up in the water, they cause a clash with the laminar boundary condition in Stokes Law, leading several scholars to adjust Stokes Law to larger particle Reynolds

numbers.

Some research has been performed on the topic of settling behavior in dredging plumes, but the amount is limited. Spearman et al. (2020) conducted in-situ experiments of deep sea mining plumes and highlighted the reduction of plume dispersal by the effects of flocculation. Mikkelsen and Pejrup (2001) examined in-situ Particle Size Distributions (PSDs) measured by A LISST-100x along a dredging plume and showed the occurrence of floc formation in the plume. Smith and Friedrichs (2011) conducted a field experiment with a Particle Imaging Camera System (PICS) and Acoustic Doppler Current Profiler (ADCP) to quantify aggregate states and flocculation in a dredge plume. The plume consisted of silt (46 %), clay (53 %) and sand (16 %). The results showed that $20\% - 50\%$ of the total sample mass consisted of bed aggregates, and $50\% - 80\%$ of flocs. Particle sizes ranged from 30 to 70 μm for primary particles, from 40 to 200 μm for bed aggregates, and from 40 to 800 μm for flocs. Median settling velocities ranged from 0.8 to 1.7 mm/s. It was also shown that the vertical mass flux in the passive phase of the plume was dominated by flocs.

Deposition and re-suspension
Once particles have reached the seabed, the processes of deposition and re(suspension) come into play. They are discussed in this sub-section about the passive far-field, but play a role in the near-field as well. Both processes take place at the seabed-water interface. The balance between the two results in the net mass flux across the interface:

$$J = E - D \tag{2.4}$$

where:

J = vertical mass flux
E = resuspension rate
D = deposition rate

A common parameterization of the deposition rates of cohesive sediments, attributed to Krone, is given here as Equation 2.5, (Krone, 1962, as cited in Sun et al., 2016).

$$D = w_s C \left(1 - \frac{\tau_b}{\tau_d}\right) \tag{2.5}$$

where:

τ_b = bottom shear stress
τ_d = critical shear stress for deposition

After particles have deposited, they can be (re)suspended by the flow of water above the seabed. Equation 2.6 gives a formulation for the linear (re)suspension rate. Krone refers to this formulation as 'Kandiah's relation' (Krone, 1999, as cited in Van Prooijen and Winterwerp (2010). Both Van Prooijen and Winterwerp (2010) and Sun et al. (2016) follow Krone in attributing this formulation to Kandiah.

$$E = M\left(\tau_b - \tau_c\right) \tag{2.6}$$

where:

τ_c = critical shear stress for (re)suspension
M = model parameter

The authors note that there are two main paradigms relating to the processes of deposition and reposition. The first assumes that, depending on the shear stress, only one of these processes takes place; the second assumes that deposition and resuspension take place simultaneously. The latter paradigm appears to have gained the most popularity.

2.1.3. Transition

Having discussed the dominating processes in the near-field and the far-field, we will now focus on the transition between these two areas. At the transition, buoyancy effects diminish and mixing is taken over by turbulence generated by the ambient water. Where and when this occurs, is different for every plume. From the previous sections it is clear that this depends on the characteristics of the sediment, the operational conditions and the local conditions. Kemps and Masini (2017) point out that the transition occurs in the initial stage for some plumes, and (to a greater or lesser extent) in a later stage for other plumes, when impacting the seafloor and/or after being spread across the bed. In any case, with time, all plumes become more passive until they have become completely passive. In the literature, there appears to be a general consensus that the far-field – the region where the complete plume shows passive behavior – starts at a few hundred meters from the vessel (e.g. Spearman et al. 2007, Becker et al., 2015).

Determining where the transition occurs is mainly relevant for modelling reasons. Processes in the near-field and the far-field take place on such different scales in time and space, that different sub-models are needed to cover the whole trajectory of the plume. Source terms are used to describe the characteristics of the plume at the end of the near-field. This information is subsequently used as input in the far-field (sub)model. In order to find a metric for the end of the near-field, a condition must be found that defines the end of the dynamic phase. In the literature there is no consensus on this. De Wit (2010) introduces the so-called local plume Richardson number Ri_l , defined in Equation 2.7, as a candidate for a transition parameter. The method suggests that when the local Richardson number is below 0.15, buoyancy effects have diminished and mixing is taken over by the ambient current.

$$Ri_l = \frac{g\Delta\rho_l/\rho_a D_l}{u_{cf}^2} < 0.15 \tag{2.7}$$

where:

$\Delta\rho_l = \rho_l - \rho_a$
ρ_l = local centerline density of the plume
D_l = local plume width, defined by a top hat profile

D_l can be calculated using the principle of conservation of plume volume, see Equation 2.8. The implicit assumption when using this equation is that all sediment is (still) in suspension.

$$C_l \frac{\pi}{4} D_l^2 U_l = C_0 \frac{\pi}{4} D_0^2 W_0 \tag{2.8}$$

where:

C_l = center line plume concentration
U_l = center line plume velocity
C_0 = initial plume concentration
D_0 = initial plume diameter

Using the transition parameter described above, De Wit (2010) carried out CFD simulations to determine the transition depth. This is the depth at which crossflow drive behavior becomes dominant. The transition parameter does require center line properties as input, such as the center line density, velocity and concentration. It is therefore not equipped to determine the transition when no CFD modelling has been performed. Also, although useful for gaining insight into the effect of water depth on plume behavior, the approach taken by De Wit (2010) does not easily translate into information on the horizontal location of the transition.

2.1.4. Source Term Estimation

Far-field modelling requires an estimate of a far-field source term and a decision on where to implement it. According to Kemps and Masini (2017), carrying out a proper field data collection program

during dredging trials in the area where dredging is to take place gives the best chance of obtaining a realistic source term, however, since this is a very costly and complex exercise, it is seldom carried out.

According to Lisi et al. (2019), there are two main methods to estimate the source term. The first approach entails detailing the near-field regime with the help of a Computational Fluid Mechanics framework, and thus gain insight in the dynamics of the sediment moving into the far-field. Disadvantages are the cost and the fact that the result is not generalizable. Alternatively, a macro-scale modelling approach can be taken. This refers to empirical or conceptual models. Conceptual models base the source term on various parameters related to the characteristics of the site and the dredging operations.

Becker et al. (2015) describe a generic approach for source term estimation based on current best practice. The approach does not involve modelling of near-field processes, which makes it attractive to use. The estimation starts with a calculation of the amount of fines (in kg) that is available from the dredged material. Subsequently, this mass is distributed over the different work methods that are used. This is done by applying source term fractions. These fractions link the amount of suspended fine particles to the amount of fine particles in the soil and the dredge methods used.

The authors stress that it is good practice to check the applicability of the fractions with field measurements for the specific project; great care must be taken with fractions not based on proper measurements. Having expressed these words of caution, Becker et al. (2015) present reasonable ranges for various source term fractions. For the overflow source term fraction – the fraction of the amount of fines leaving the overflow that is transported to the far-field – 0-20% is presented as a reasonable range.

Van Koningsveld (personal communications, 19 April, 2022), explains how this range was arrived at. First, (hundreds of) measurements were carried out in the vicinity of a dredging vessel in operation. Use was made of an ADCP; for verification purposes, data was also collected from 3 OBSs (Optical Backscatter Sensors) and water samples. The data was collected along the following tracks: 1 track upstream from the ship laterally across the current (background information), 4 to 5 tracks downstream laterally across the current, and 1 track towards the ship through the heart of the plume. For the downstream tracks, average flow velocities and the total flux over the water column were calculated. Combining this with the current velocity, the age of the plume was calculated. Plume age (x-axis) and total flux (y-axis) were subsequently put in a graph. These graphs showed that the total flux diminished more initially and slower after a certain plume age. This change was seen as the transition. The flux at that point divided by the flux at the overflow was labelled the source term fraction. Van Koningsveld (personal communications, 19 April 2022) notes that ranges of source term fractions were presented because the transition is not very sharp.

As mentioned above, the water velocity and discharge measurements that Becker et al. (2015) used for determining realistic source term ranges were collected with an ADCP. A brief description of this system is given here, because the method has certain limitations which are relevant when interpreting the results. Mueller et al. (2007) explain that an ACDP is an instrument that is based on the Doppler principle: an acoustic signal is reflected by small particles in the water. The transducer that emits and receives the acoustic signals can be mounted on a boat; 3 or 4 beams are pointing at an angle into the water. One of the limitations of this method is that there is a so-called blanking zone at the water surface, where measurements are impossible to take. In addition, there is a zone near the bed where an ADCP is prone to make errors. The reason is that the system has side lobes that are emitted at an angle from the main beam. These side lobes can interfere with signals emitted from the main beam. These erroneous measurements can affect 6% to 13% of the water column. Van Eekelen (personal communications, 7 September 2022) and Van Koningsveld (personal communications, 5 September 2022), co-authors of the study by Becker et al. (2015), acknowledge that ADCP measurements are incomplete or imprecise in the above mentioned parts of the water column, but the authors both still have faith in the realistic ranges for the source term fraction as presented in the study by Becker et al. (2015). Van

Eekelen notes that the realistic ranges have been discussed with various experts, and Van Koningsveld does not expect the missing information to have a large effect, adding that the source term fraction value for a certain dredging project can be adjusted anyway after carrying out characterization monitoring at the start of a project.

Notwithstanding these assurances, the fact remains that accurate measurements in the zones mentioned above cannot be obtained with an ADCP. As a consequence, (part of) the sediment in these zones may not be included in the Becker source term fraction of 0-20%. One of the objectives of this study is to study the near-bed zone, by using a numerical model to study the vertical distribution of sediment in overflow plumes.

2.2. Literature review

In Section 2.1, about background theory, a range of studies by other authors was referred to. This section looks closer at (a selection of) this literature. Section 2.2.1 briefly discusses the (shift in) research methods used over the years. Section 2.2.2. zooms in on relevant research studies carried out in the past 15 years, by discussing a selection of these studies in chronological order.

2.2.1. Research Methods

Turbulent jets in a cross-flow were initially studied by conducting theoretical research, based on the continuity and momentum equations. Over time, the research field made steady progress thanks to new insights, for example on the roles of the Richardson number and the velocity ratio, but solutions were approximate and could not capture the complete process of flow development. The supplemental use of measurements led to improved results, but solutions were still incomplete. In recent years, numerical simulation has become an important approach, thanks to progress in the fields of computational fluid dynamics, vortex motion theory and turbulence models (Chen et al., 2022). Through numerical modelling, the effects of dredging can be predicted, without conducting expensive full-scale trials (Stewart & Leaman, 2013).

2.2.2. Literature

In recent decades a number of studies into dredging induced sediment plumes have appeared. Although (concerns about) the environmental impact of these plumes is mentioned in most publications, this does not appear to have led to a large body of literature on dredge plumes (yet).

Spearman et al. (2006) developed a process based dispersion model of a THSD. The model consists of sub-models for the processes in the hopper and for the descent and collapse of the dynamic plume, and also has a sub-model for the passive plume. The authors quite rightly point out that this is not a simple task, given the very different length and time scales in the dynamic and the passive phase. The source terms are determined both in terms of magnitude and shape, and are passed to the sub-model of the passive plume where sediment particles are tracked in 3D over time and space. Existing laboratory data were used for validation of the model. Although appropriate field data for validation were still lacking, tests suggested a promising performance. If nothing else, the fact that the model covers both the dynamic and passive phases as well as the connection between them, sets the model apart from most other models and is promising in itself.

In a study on far-field dredge plume dispersion, Tuinhof (2014) conducted a literature study to identify parameters that affect dispersion. He found three types: model, ambient and input parameters. Using Delft3D-FLOW (a software engine), experiments were carried out to test the effects of the various pa-

rameters. The results were subsequently compared with field measurements. It was found that it is not appropriate to use a virtual source at the location of dredging. Rather, the near- and the far-field should be coupled through a source term. The study further showed that the lateral and vertical distribution of the source term have an effect on the sediment concentration and the far-field fluxes respectively. Under the conditions studied, the author noted that implementing a source term in a single grid cell with a grid size of 50 m, whilst the actual plume width is 500 m, leads to a factor 10 overestimation of the peak concentration in the far-field.

De Wit (2015) studied the behavior of TSHD sediment plumes in the near-field. Focusing on the overflow plume within a few hundred meters of the vessel, De Wit used a combination of CFD model simulations in 3D, experiments, and measurements (laboratory scale and full scale) to validate the model. One of the main contributions of the study lies in a better understanding of the vertical distribution of the plume, including the formation of a surface plume. Another contribution are the guidelines for determining a far-field source flux. Generally, the flux after approximately 15 minutes plume development is appropriate for using as a far-field source, in the opinion of the author. The author judges that the density difference after 15 minutes is no longer important.

Decrop and Sas (2018) studied near-field plume dynamics to improve knowledge about the horizontal and vertical distribution of sediment going into the far-field. The author used a stepwise approach that started with laboratory-scale experiments. Then, a corresponding CFD model was built, and the results of the model were compared with the results of the experiments. After resizing the model to prototype-scale, field measurements were collected to validate this resized model. This was followed by simulations carried out to identify the effect of (changed) conditions on the near-field plume. Finally, a model was built that captured the non-linear interactions between the influencing factors. The model's predictions of the vertical distribution of the sediment flux were shown to be relatively accurate.

All three studies described above use field data to validate the numerical models. Although this is important for increasing the accuracy of the models, it can be a challenge in practice. As Sun et al. (2016) point out, data availability can be a problem, especially at the EIA stage. The data should be collected over various seasons and locations to account for variations in time and space. In cases where this is not possible, the authors advise to use existing data from a similar location, if available. According to Kemps and Masini (2017), collecting data during preliminary dredging trials gives the best chance of obtaining realistic source term estimates. They acknowledge, however, that such trials are expensive and logistically complex.

Taherian and Mohammadian (2021) conducted a review study to better understand buoyant jets in crossflows, with the ulterior goal of improving the management of discharges and limiting the negative effects on marine biota. The study looked at effluent discharges such as brine or thermal discharge. In that context, mixing and dispersion of the effluent are seen as something positive. The main focus of the study was on the mixing capabilities of buoyant jets, which are not well understood yet, according to the authors, due to the complex fluid interactions and dispersion behavior of such jets. The research zoomed in on the various vortical structures that form in buoyant jets in crossflows, including a counter-rotating vortex pair. These structures are believed to explain the mixing capabilities of buoyant jets in crossflow. Since the authors not merely present a summary of existing studies, but also weave all the results to a coherent story, this study offers an important contribution to the understanding of buoyant jets in crossflows.

Chen et al. (2022) very recently developed an advection and diffusion model of the TSHD overflow. The authors applied the widely used LES method in combination with the volume of fluid method (VOF) to gain insight into the effect of various internal and external factors on overflow regimes. The internal factors in this study were the Richardson number and the velocity ratio. External factors were the structure of the hull tail of the vessel, the position and frequency of the overflow, and the propeller. Comparison with existing experimental data showed that the model performed well. With regard to

the internal factors, the study showed that a low Ri and/or a high ζ flow are inducive for (the environmentally damaging) surface plumes. External factors shown to cause more surface plumes are the propeller and the structure of the hull tail, because they lead to increased turbulence.

De Wit et al. (2022) used CFD 3D modelling to study the overflow spill available for far-field dispersion as a result of CSD loading a stationary hopper barge. The authors study and analyze the filling of the barge, the flux from the overflow, and the sediment from the overflow available for dispersion in the far-field. The resulting far-field source term is compared to the source term resulting from following the empirical approach proposed by Becker et al. (2015). In their simulation study, De Wit et al. (2022) covered three expected particle size distributions, by varying the loading characteristics. They also covered three different ambient current velocities:. 0.1, 0.2 and 0.5m/s. Far-field source terms were generated for three different plume ages, at 15, 30 and 60 minutes from the source. The study showed that the source terms at 30 and 60 minutes from the source were comparable to the source terms when using the Becker method. The study further showed that the particle size distribution mainly influenced the mass fraction exiting the overflow barge; the ambient current velocity was the main factor influencing subsequent deposition.

2.3. Conclusion and knowledge gap

Section 2.2 shows that the body of research on the prediction of TSHD dredge plumes in the far-field has continually grown over the past few decades. This has led to a basic understanding of the behavior of the dredge plume: how it leaves the overflow under the influence of momentum, how the Richardson number and velocity ratio determine the subsequent regime (density-driven vs. buoyancy-driven), how the formation of a surface plume comes about, and how the plume changes from dynamic behavior of the plume to passive behavior.

As described in Section 1.3.2, far-field dredge plume predictions are typically made with the help of numerical models such as Delft3D. These models require a source term as input, reflecting the magnitude and characteristics of the dredge plume as it enters the far-field. The proper determination and implementation of this source term is very much an area of active research. The source term fraction method (and the realistic range for this fraction) proposed by Becker et al. (2015) is a popular approach, but characterization measurements to refine the realistic range for specific dredging operations are not always carried out. Furthermore, Becker et al. (2015) do not elaborate on where (at which distance) the reasonable ranges for the STF can be expected (and therefore where they should be implemented). The magnitude of the source term (fraction) and its implementation (vertical and lateral distribution of sediment in the plume, and the implementation location) are often based on assumptions. If these assumptions are misguided, this will result in wrong predictions.

A more informed use of the source term and the source term fraction concept would improve the quality of far-field dredge plume predictions. This thesis aims to fill this gap. Building on existing knowledge about relevant external conditions influencing TSHD dredge plumes, a numerical simulation study was carried out with the aim of finding out the effect of (combinations of) typical conditions on the development of the plume, on its vertical and lateral distribution (shown by several authors to be important) and on where to implement it. Special attention is paid to the part of the plume that is present in the bottom 6% - 13% of the water column, since that part cannot be accurately measured by ADCP measurements. The insights into this near-bed plume can be used to supplement field data collected by ADCP; they also provide an estimate of the amount of sediment that is possibly not (completely) included in the realistic range as proposed by Becker et al. (2015). The next chapter, Methodology, explains the chosen approach in more detail.

3

Methodology

The body of knowledge about implementing TSHD source terms on the far-field computational grid in an appropriate manner is limited. As described in the research objective in Section 1.4 this research aims to support a more informed implementation of TSHD source terms on the far-field computational grid. Regarding source terms, there is a lack of knowledge on how to determine important aspects such as:

- *What is the amount of suspended sediment entering the far-field?*
- *How should the source term be distributed vertically and laterally on the far-field computational grid?*
- *Where should the source term be implemented on the far-field computational grid?*

A numerical scenario study with a validated 3D CFD model was carried out. This methodology was selected for two main reasons. Firstly because the LES (Large Eddy Simulation) approach, which is at the basis of the CFD model that is used, has the ability to solve for the highly turbulent flow in the vicinity of the TSHD. The relevant processes in the dynamic phase of the plume are thereby adequately captured. Secondly, this methodology was selected because of the opportunity it offers to study the behaviour of the plume under various conditions. By conducting multiple model runs under various conditions, a rich set of data can be analyzed and used to form recommendations regarding the aspects mentioned above.

The resulting model output of the individual model runs are evaluated in terms of dredge plume character and magnitude. The magnitude of the plume is evaluated during various stages of plume development by assessing the sediment fluxes. Subsequently, the simulated sediment fluxes can be compared to the reasonable range as presented by Becker et al. (2015). TUDflow3D is a trusted and well-calibrated tool for the prediction of the fate and development of TSHD dredge plumes in the near-field. De Wit et al. (2014) was one of the first who compared field measurements in the immediate vicinity of the dredger with simulations performed with TUDflow3d. TUDflow3d reproduced the field measurements in a satisfactory way.

3.1. TUDflow3D

TUDflow3D is a fully three dimensional solver which can give detailed results of turbulent flows on engineering scale. It has been developed for performing simulations of TSHD overflow plumes in the dynamic near-field. It has been validated with lab measurements and field measurements (De Wit, 2015). In this section, the governing equations of the model are described.

3.1.1. Flow

The Navier-Stokes equations describe the conservation of momentum and mass for fluid motion. TUDflow3D solves the variable density incompressible flow Navier-Stokes equations.

$$\begin{aligned} &\frac{\partial \rho}{\partial t} + \nabla \cdot (\rho u) = 0 \\ &\frac{\partial \rho u}{\partial t} + \nabla \cdot (\rho u \otimes u) = -\nabla P + \nabla \cdot \tau + (\rho - \rho_a)\, g, \end{aligned} \tag{3.1}$$

where:

ρ = mixture density
u = fluid velocity vector
t = time
P = dynamic pressure
τ = viscous shear stress

The mixture density ρ is computed at each location of the grid following Equation 3.2.

$$\rho = \rho_a + \sum_{l=1}^{nfrac} C_l \, (\rho_l - \rho_a) \tag{3.2}$$

where:

C_l = volume concentration for each fraction
ρ_l = density of individual fraction

By using a variable density, TUDflow3D is able to capture the general negatively buoyant JICF behavior of the overflow plume under the keel of the TSHD. TUDflow3D typically uses a radially spreading ('pie-shaped') cylindrical grid (r, ϕ, z), see Figure 3.1. This is an efficient grid choice, as the grid shape follows the lateral spreading of the plume. The grid is equidistant in ϕ and z direction and variable in r direction. This structured grid allows for the use of a structured solver, which is more (cost-) efficient than its unstructured counterpart.

3.1.2. Turbulence

The majority of flows found in nature are turbulent flows: they can be characterized by high Reynolds numbers (high Re: high ratio of inertial to viscous forces). Turbulence is an important three-dimensional and rotational phenomenon. Turbulent motion transfers momentum, mass, energy and heat at a higher rate than molecular motions. Turbulence is a three-dimensional phenomenon, infamous for its large range of scales that must be resolved. The most accurate method of resolving turbulence in all its complexity is Direct Numerical Simulation (DNS). As the name suggests, DNS numerically solves the full Navier-Stokes equations on a fine grid capturing all scales present in the flow in question. Such direct numerical simulation is typically only computationally feasible when applied to flows with low Reynolds numbers. When DNS is not feasible, turbulence can be represented in the Navier-Stokes equations by means of an eddy viscosity ν_e, see Equation 3.3. Equation 3.3 shows the constitutive expression for the stress tensor τ in Equation 3.1.

$$\tau = \rho v_e \left(\nabla \boldsymbol{u} + \nabla (\boldsymbol{u})^T - 2/3 \nabla \cdot \boldsymbol{u} \right) \tag{3.3}$$

where:

ν_e = eddy viscosity

This eddy viscosity ν_e is the sum of the molecular viscosity ν_{mol} and the so-called turbulent viscosity ν_t. The eddy viscosity concept is based on the idea that turbulent eddies transfer momentum in a

similar way as momentum transfer caused by molecular diffusion. The hypothesis that the transfer of momentum caused by turbulence can represented in a model by introducing a turbulent viscosity ν_t analogous to a molecular viscosity ν_{mol} is referred to as the Boussinesq approximation.

There are different types of turbulence models that make use of the eddy viscosity concept, with varying degrees of complexity. In TUDflow3D, turbulence is captured by use of 'Large Eddy Simulation'(LES). LES relies on the solving of the large eddies, which contain the majority of the turbulent kinetic energy, directly. The small scale turbulence, mainly responsible for the withdrawal of energy from the large scale motion, takes place on smaller scales than the spatial filter (=grid size) and is not solved directly. The effects of the small scale turbulence are accounted for through a sub-grid model: $\nu_t = \nu_{sgs}$. TUDflow3D makes use of the WALE (Wall Adapted Local Eddy viscosity) model as a sub-grid-scale model, which is designed to return the correct wall asymptotic behaviour for wall bounded flows.

3.1.3. Sediment dynamics

A multi-fraction approach is used in TUDflow3D to model sediment. Any sediment that is dredged has a Particle Size Distribution (PSD). A PSD can represented in the model by a number of sediment fractions. Each fraction is assigned characteristics such as particle diameter, settling velocity and density.

Settling dynamics
In Chapter 2 the settling velocity of particles in the Stokes regime was presented. In Section 2.1, the relevance of the phenomenon of flocculation was also highlighted. Flocculation, the aggregation of cohesive sediment to form flocs as a result of cohesive forces, has been shown to play an important role in the settling dynamics of dredge plumes by Smith and Friedrichs (2011). The effect of flocculation can be included in TUDflow3D simulation by introducing a floc diameter D_f and a corresponding 'floc' settling velocity $w_{0,f}$. Equation 3.4 which is used in TUDflow3D to calculate this $w_{0,f}$ has been presented by Winterwerp (1999).

$$w_{0,f} = \frac{\alpha}{\beta} \frac{\Delta\rho/\rho g D_p^{3-n_f}}{18v} \frac{D_f^{n_f-1}}{1 + 0.15 Re_f^{0.687}} \tag{3.4}$$

where:

D_p = particle diameter
D_f = floc diameter
$\Delta\rho$ = difference in mud particle density and water density
$Re_f = \frac{w_{0,f} D_f}{v}$

Transport of sediment
Equation 3.5 shows the transport equation implemented in TUDflow3d that accounts for the transport of sand, mud and air.

$$\frac{\partial C_l}{\partial t} + \nabla \cdot (\boldsymbol{u}_l C_l) = \nabla \cdot (\Gamma \nabla C_l) \tag{3.5}$$

where:

Γ = diffusion coefficient

In the vertical, sediment is transported by the mixture velocity, corrected with a drift velocity to account for settling. The drift velocity is the settling velocity corrected for the return flow created by all settling fractions. This approach was introduced by Manninen et al. (1996). In the horizontal, the mixture velocity transports sediment.

Interaction with the bed
In Chapter 2, the classical deposition function for mud by Krone was introduced. The deposition function implemented in TUDflow3D, shown in Equation 3.6 differs from Equation 2.5, as there is no critical bed shear stress for deposition. De Wit (2015) made this choice based on Winterwerp's (2007) reasoning that such a critical shear stress does not exist.

$$D = C\rho w_s \tag{3.6}$$

The erosion of fines from the bed does follow the formulation of the erosion flux as presented in Equation 2.6.

3.1.4. Implementation TSHD

A schematized shape of a TSHD is included in the model by a direct forcing immersed boundary method. The vessel's dragheads and suction pipes are also included as obstacles. TUDflow3D also accounts for the (strong) flow generated by the TSHD's propellors by using a body force source term in the momentum equations.

3.2. Model set-up TUDFlow3d

In this section the model set-up of TUDflow3D is discussed, including important assumptions and the reasoning behind the choice of scenarios that are included in this research.

3.2.1. Extension to 60 minutes plume development

Initially, the first 350 meters of plume development are simulated for each scenario on a cylindrical grid, with LES. To obtain a more comprehensive picture of the fate of the plume, 27 more simulations are performed with TUDflow3D, but with a coarser model settings. This is executed in a similar manner as performed by De Wit (2015). The (time-averaged) model output at the end of the 350 m is used as inflow boundary conditions of the simplified extended model with a coarser grid and a simplified turbulence model.

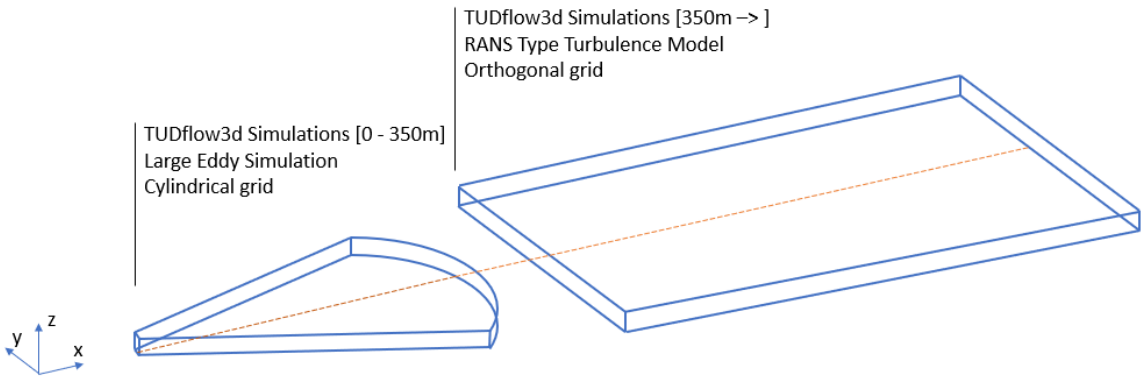

Figure 3.1: Visualization of TUDflow3D grid for the detailed LES simulation and the subsequent extended model

This extended model simulates up until 60 minutes of plume development. The main differences between the extended model solver and the 'near-field' solver are:

- A coarser Cartesian orthogonal grid .
- RANS type mixing length model.

The extended model solves the Reynolds Averaged Navier-Stokes (RANS) equation. Again, the Boussinesq approximation is applied. The turbulent stresses are calculated in a similar way as the for the LES approach: the turbulent viscosity ν_t is the result of multiplying a length scale with a shear term. However, for this model, the vertical length scale is given by the Bakhmetev profiel and the shear term is based on the RANS-time-averaged velocities in the extended model.

3.2.2. Base case

The base case consists of a 150-metre-long trailing suction hopper dredger with a draught of 8 metres. The round overflow pipe has a diameter of 2.25 metres and the overflow discharge is 7 m^3s. The overflow discharge consists of a sand-mud-water mixture with entrained air. The overflow discharge is not fluctuating in time and there is 4% air entrainment in the overflow shaft; this is kept constant for all runs. The ambient current is constant in time and directly against the sailing direction of the TSHD. The TSHD has constant sailing speed of 0.75 m/s

The sediment present in the mixture is represented by two fractions: a fine mud fraction with a particle size $D_p = 32\mu m$ and a coarse sand fraction with a particle size $D_p = 220\mu m$. A degree of flocculation is assumed for the mud fraction based. This degree of flocculation is kept constant in the scenario study. As mentioned earlier, flocculation is taken into account in the model by adjusting the settling velocity to a floc settling velocity. In all simulations for this research, flocculation is taken into account by choosing a floc diameter $D_f = 5D_p$; five times the particle diameter. The resulting settling velocities are:

- Fines $w_s = 0.0035$ m/s
- Sand $w_s = 0.0226$ m/s

3.2.3. Scenarios

A simulation study consisting of 27 runs was carried out. This number of runs was the result of varying the values of three different input parameters which reflect (some of the) external conditions under which dredging can take place. For each parameter, three different values were chosen. The 27 runs represent all possible combinations of the three parameters taking on three different values (3x3x3=27) in this numerical lab. The aim was to gain insight in the effects of the different (combinations of) external conditions on the development of the plume, as basis for a more informed use of the far-field source term and source term fraction.

The choice is made to vary three parameters. For the scenario study, the following parameters are included:

- Dredging depth d
- Effective flow velocity u_{cf}
- Overflow density $\rho_{overflow}$

These parameters were chosen because of their shown or expected importance for dredge plume development. Decrop and Sas (2018) showed the relevance of dredging depth; De Wit, Bliek and Van Rhee (2020) showed the relevance of effective flow velocity (this is the combined effect of sailing speed and ambient current, also called crossflow velocity). Mixture density was chosen because it represents different phases of overflowing. It is also part of the equation for the Richardson number, and as such can be expected to have an effect on plume development. For all three parameters, a range of three

realistic values was selected on the basis of existing work (e.g. De Wit, Bliek, 2020; Van Rhee, 2020). The following values were chosen:

- Dredging depth d: 15, 20 and 25 m
- Effective flow velocity u_{cf}: 0.75, 1.25 and 1.5 m/s
- Overflow density $\rho_{overflow}$: 1100, 1200 and 1300 kg/m^3

Figure 3.2 shows an overview of the conditions for each of the 27 runs.

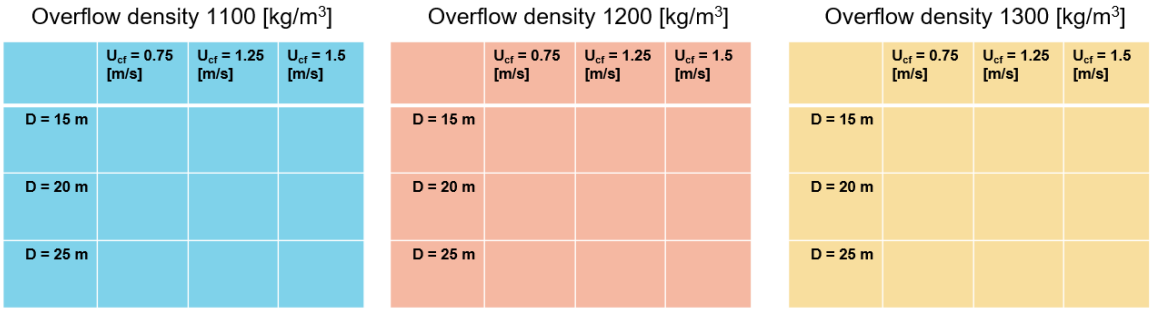

Figure 3.2: Overview 27 simulations and the varying conditions

The values for the effective flow velocity are achieved by varying the ambient current: $u_{cf} = u_{tshd} + u_a$. For the ambient current, velocities of 0, 0.5 and 0.75 m/s are selected. In combination with the constant sailing speed of 0.75 m/s, this results in the effective flow velocities mentioned above, see Table 3.1.

	u_{cf} = *0.75 (m/s)*	u_{cf} = *1.25 (m/s)*	u_{cf} = *1.5 (m/s)*
Sailing speed u_{tshd} *(m/s)*	0.75	0.75	0.75
Ambient current u_a *(m/s)*	0	0.5	0.75

Table 3.1: Chosen ambient current velocities, sailing speeds and the resulting crossflow velocities

For each of the three densities, a different ratio fines/sand is assumed. Different overflow densities represent different stages of overflowing„ where 1100 kg/m^3 represents the beginning phase, where mainly fines are making up the sediment in the overflow. As the overflowing progresses, the overflow mixture will contain more and more sand. It is assumed that during the final phase of overflowing (1300 kg/m^3) nearly half of the sediment in overflow consists of fines.

Mixture density	*1100 kg/m3*	*1200 kg/m3*	*1300 kg/m3*
Volume fraction: fines	0.0432	0.0734	0.08
Volume fraction: sand	-	0.0315	0.086

Table 3.2: Volume concentrations for each sediment fraction for different mixture densities

Figure 3.3 shows an overview of the most important input parameters of the model. Highlighted are the parameters that are included in the scenario study as well as the parameters that are adjusted for the simplified runs (the 60 minute simulations).

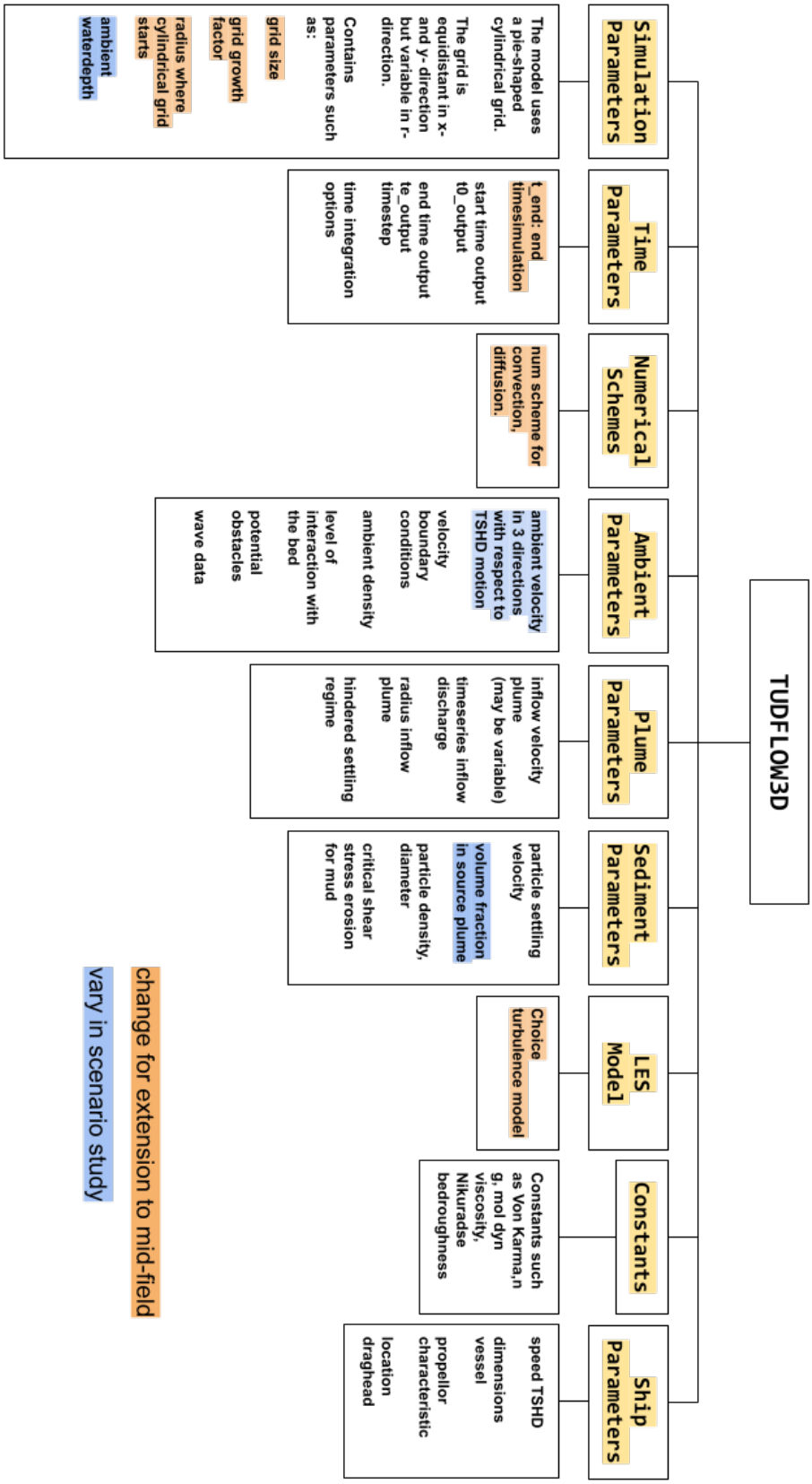

Figure 3.3: Overview all input parameters TUDFlow3d

4

Results and Analysis

In this chapter, the results of the simulation are presented, both graphically and in words. Throughout the chapter, the results are also analyzed. This is done by interpreting the results in the light of the processes described in Chapter 2. Because of the wealth of data, only the main findings are included in this chapter. Additional graphs have been placed in the Appendices.

4.1. Magnitude of the plume

This section describes the results of the simulation runs with regard to the magnitude of the plume. First for fines, then for sand. To give the reader an impression of the simulated plume, Figure 4.1 shows an isosurface, plotted at an arbitrary concentration of 50 mg/L. The contours of the cylindrical grid are visible and the contours of the aft of the vessel (up until x = 100 m).

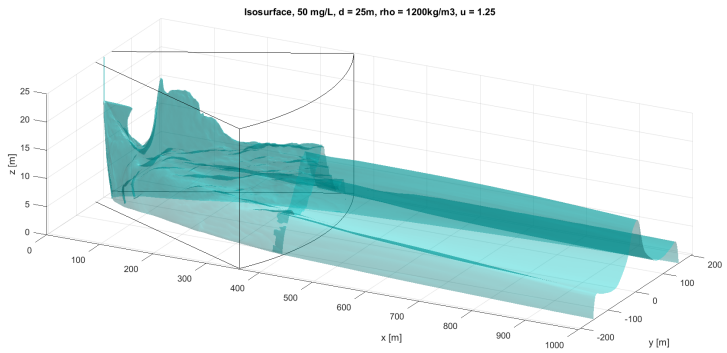

Figure 4.1: 3D Isosurface at 50 mg/L for an individual simulation.

4.1.1. The magnitude of the fines plume

In order to get a first, birds eye view of the results, Figure 4.2 shows the plume age at the moment when the fines flux, as percentage of the total overflow fines flux, is 20%. Via the Y-axis, the colors and the shapes of the 27 markers, the results can be linked to the conditions that were varied in the runs. The percentage of 20% is chosen because it is equal to the (high end of the) realistic range for the source term fraction as presented by Becker et al. (2015). As mentioned in Chapter 2, this realistic range is much used in practice, but there is no general guidance on where and when the 20% occurs. This is important for a proper implementation in far-field models.

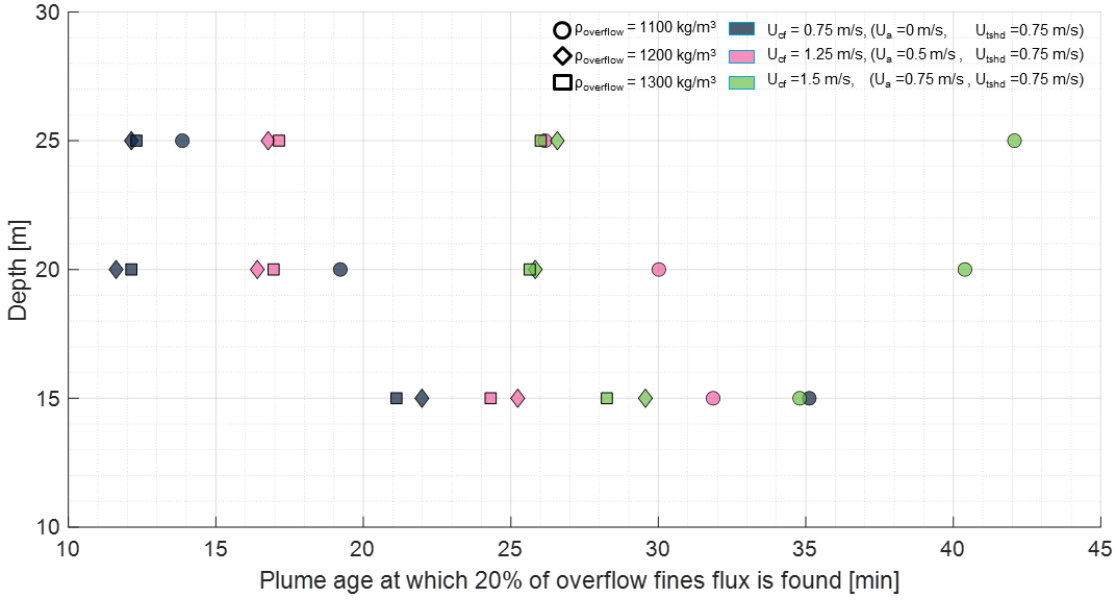

Figure 4.2: Plume ages at which 20% of overflow fines flux is found under varying conditions

Looking at Figure 4.2, we see that the plume age at the moment when the total fines flux has decreased to 20% of the overflow fines flux varies between 12 and 42 minutes, depending on the conditions. Plume age is equal to the duration of plume development.A low plume age means the sediment has been in suspension for a relatively short time. The 11-42 minutes of plume development, correspond to a distance of 0-1895 meters from the dredging location (515-3785 from the moving TSHD).

Figure 4.3 depicts above plume ages for the 27 scenarios in a different way. Figure 4.4 depicts the corresponding distances from the dredging location. Note that for scenarios with a crossflow velocity of 0.75 m/s, this distance is equal to zero. This is the result of a 0 m/s ambient current (see Table 3.1).

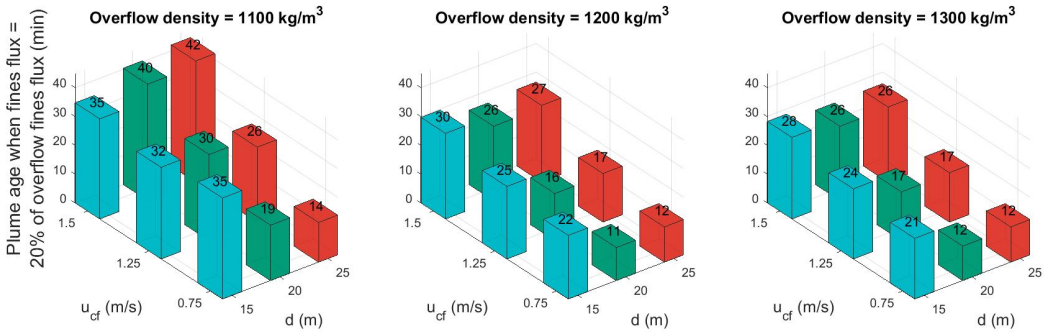

Figure 4.3: Plume ages where total fines flux = 20% of overflow fines flux

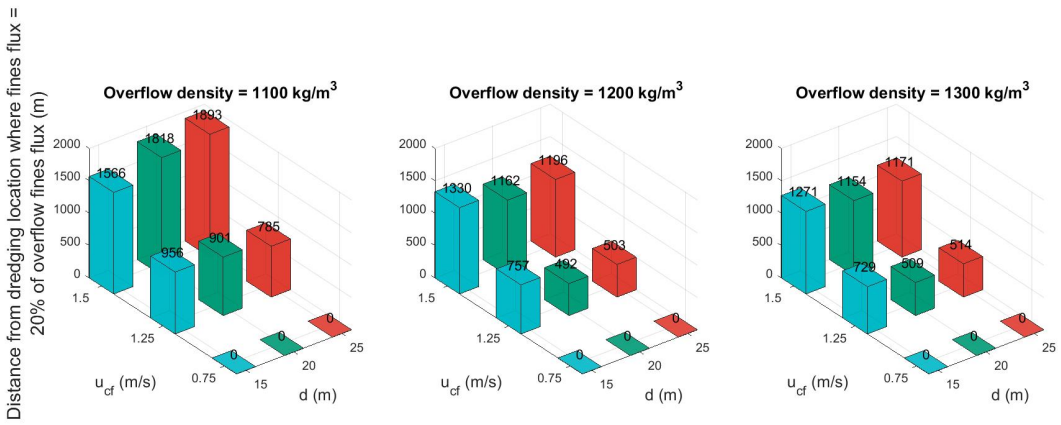

Figure 4.4: Distance from the dredging location where total fines flux = 20% of overflow fines flux for varying conditions

Looking at Figure 4.3, the following observations can be made for the moment when the total fines flux has reduced to 20% of the total overflow fines flux:

- The *highest plume ages* occur when $\rho_{overflow}$ is low (1100 kg/m^3) and u_{cf} is high ($u_{cf} = 1.5m/s$). The *lowest plume ages* occur when $\rho_{overflow}$ is higher (1200 kg/m^3 or 1300 kg/m^3), u_{cf} is low ($u_{cf} = 0.75\ m/s$) and the water is deep (25 m).

This can be explained by revisiting the Richardson number Ri and the velocity ratio ζ. A low $\rho_{overflow}$ contributes to a low Ri, and a high u_{cf} contributes to a high velocity ratio. Under those conditions, the plume is prone to mixing in the initial stages of plume development. When $\rho_{overflow}$ is higher and u_{cf} is low, the initial regime is prone to be density-driven (see Figure 2.2). Figure 4.5 and Figure 4.6 clearly illustrate these different regimes under the conditions mentioned:

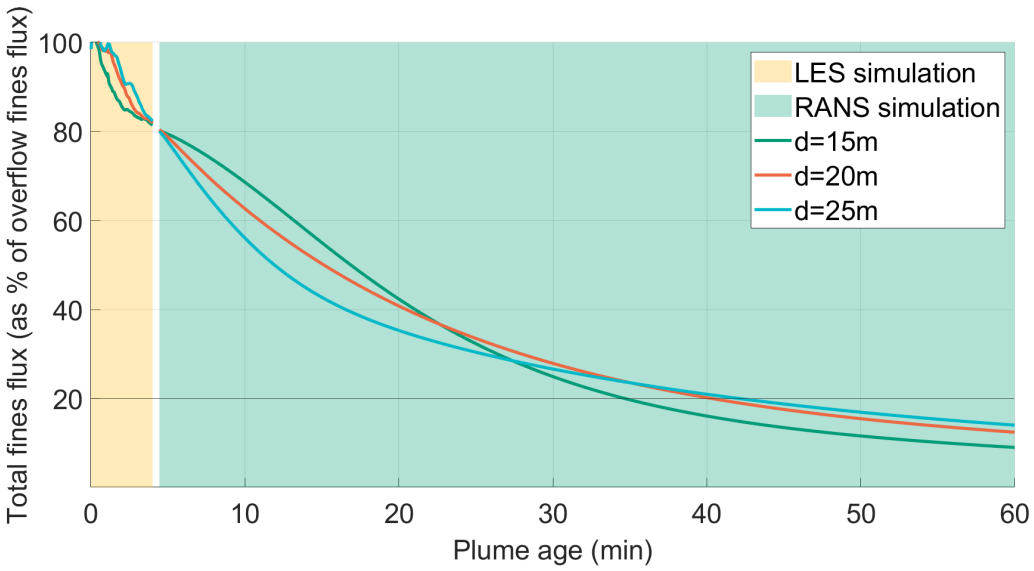

Figure 4.5: Fines flux (as % of overflow fines flux): conditions: $\rho_{overflow} = 1100\ kg/m^3$ and $u_{cf} = 1.5\ m/s$

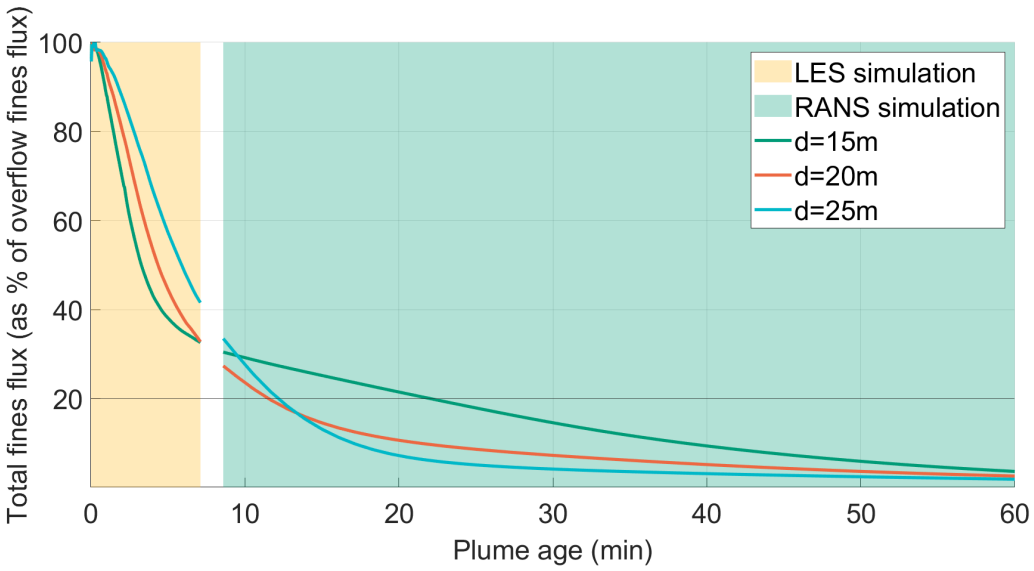

Figure 4.6: Fines flux (as % of overflow fines flux). For conditions: $\rho_{overflow} = 1200\ kg/m^3$ and $u_{cf} = 0.75\ m/s$

The left-hand side of these figures (the yellow part) shows the part of the plume that has been simulated with LES. The green part shows the subsequent (simulated with the extended TUDflow3D model) development of the % of the total fines flux up to one hour of plume development. A few observations can be made, looking at these figures. Firstly, the difference between plume development under the two sets of circumstances compared here mainly takes place in the initial phase, where density-driven behavior is present or less present. Differences in $\rho_{overflow}$ and u_{cf} explain the two different regimes; the difference in water depth only leads to modest differences in this initial phase between the three lines in each graph. Around the end of this phase, however, effects of the water depth on the % fines flux become noticeable. Figure 4.6 shows that, under conditions of high $\rho_{overflow}$ and low u_{cf}, it takes approximately twice as long for the plume to reach 20% of the overflow fines flux. This causes the line that represents shallow water conditions (depth = 15 m) to cross the other two lines after approximately 10 minutes of plume development. To gain a better understanding of what is happening here, we will look at Figure 4.7, which shows SSC cross-sections of the plume at various plume ages under the same conditions as those in Figure 4.6.

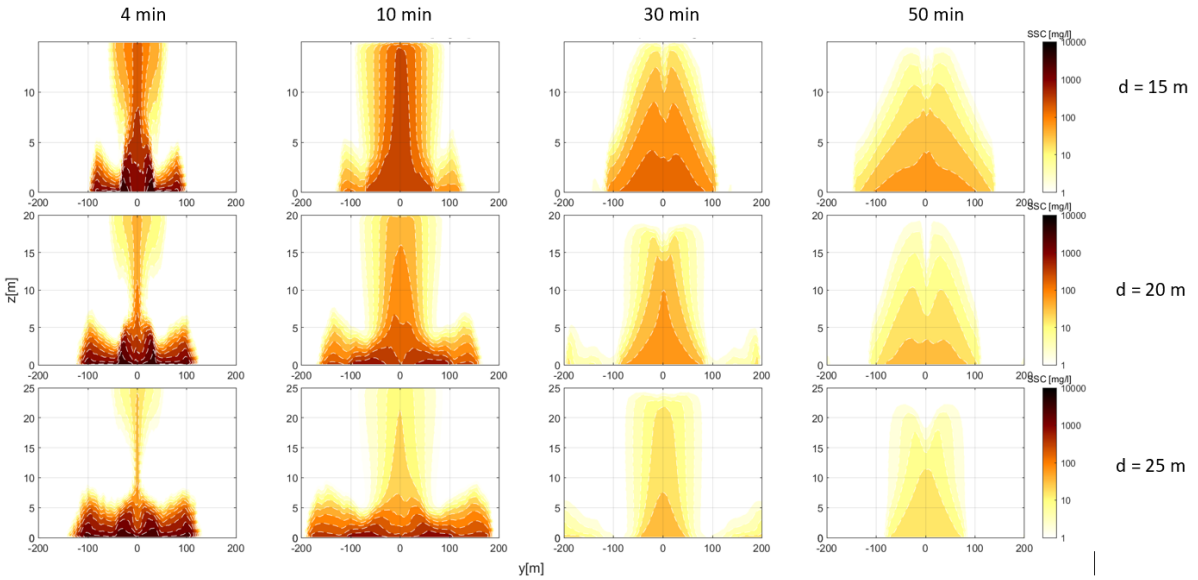

Figure 4.7: SSC cross-sections at different plume ages for depths of 15, 20 and 25 [m], respectively. Overflow density $\rho_{overflow} = 1200 kg/m^3$ and Cross-flow velocity $u_{cf} = 0.75 m/s$

Figure 4.7 reveals that the SSC of the plume develops differently for the three different water depths; this is reflected in the SSC distribution over the first 60 minutes. In all three cases, the plume shows density-driven behavior, as explained above, resulting in high sediment concentrations near the bed, but in the shallowest water (15 meter deep), another phenomenon is visible: the plume is more mixed over the entire water column, leading to higher SSC values in the top part of the water column. This can be attributed to the low keel clearance; the plume is heavily affected by the ships propeller, causing an uplift of the plume, especially in shallow water. Because of this uplift, it subsequently takes longer for the plume to settle, because it takes extra time for the uplifted sediment to reach the bed. Another possible explanation is that sediment is stripped off the density-driven plume when it impinges on the bed, subsequently mixing with the ambient water. A final possibility is that particles that already settled in the first few minutes, are re-suspended very quickly afterwards, and are transported upwards by the ambient water. The fact that a part of the sediment is moving upward from (near the) bed can also be deducted from Figure 4.8.

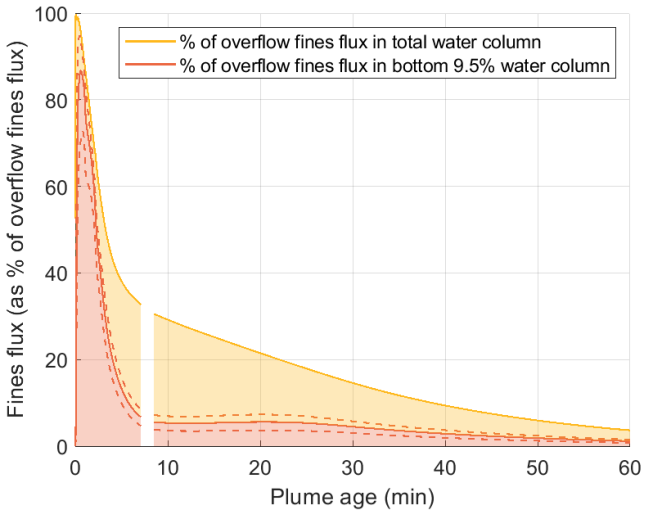

(a) Depth = 15 m

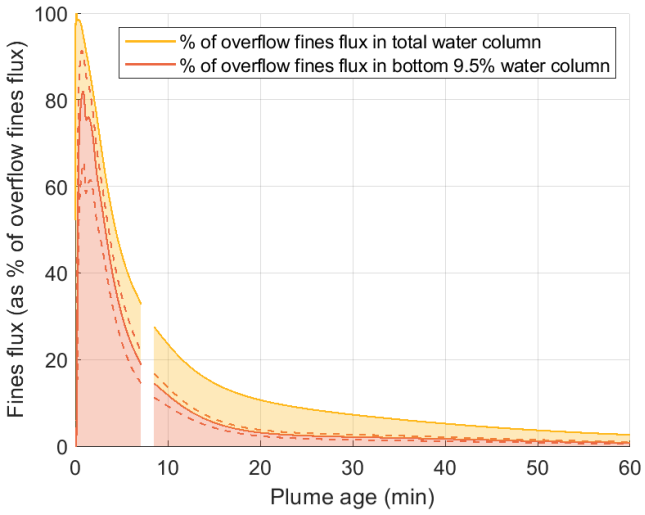

(b) Depth = 20 m

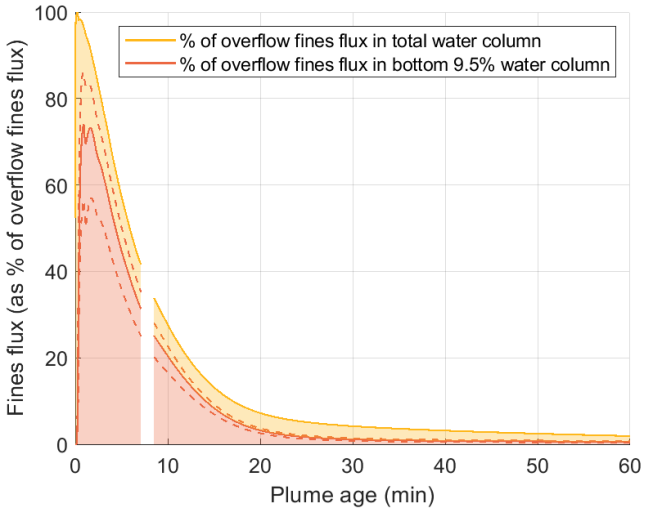

(c) Depth = 25 m

Figure 4.8: Fines flux (as % of overflow fines flux in the total water depth and the bottom 9.5 % of the water column. Dashed lines indicate a bandwith of 6% - 13 % of the water column

Figure 4.8, again, depicts the development of the flux for the 1200 kg/m^3 density and 0.75 m/s u_{cf} scenarios, for the three different water depths. The top line in each figure is the same as the line for the corresponding depth in Figure 4.6. The additional information shown in Figure 4.8, is a line that shows the percentage of the overflow fines which is present in the bottom 9.5 % of the water column. The reason for looking at the percentage of fines in this particular part of the water column is explained in Section 4.2.2. For now, suffice it to say that these figures illustrate the processes just described: that a plume with a $\rho_{overflow}$ of 1200 kg/m^3 and a u_{cf} of 0.75 m/s is lifted up in conditions of shallow water. A closer look at the three figures reveals this. Figure 4.8a, which represents the development of the plume in shallow water, shows that in the first few minutes, almost all the fines find themselves in the bottom 9.5% of the water column. Only a few percentage points of the overflow fines are present in the top 90.5% of the water column. At a plume age of approximately 8 minutes, we can see that over 20% of the overflow fines are present in the top 90.5% of the water column. This can only be caused by sediment that (temporarily) rises in the water column. Figure 4.8b shows that this effect is hardly, if at all, present in a water depth of 20 m and Figure 4.8c shows it is completely absent in water depth of 25 m.

- In *shallow water* (15m), the differences between the various scenarios are smaller than for *deeper water* (20m and 25m).

Looking at plume ages at the point when the percentage of fines has decreased to 20% of the overflow flux, Figure 4.3 shows that these plume ages vary between 21 and 35 minutes for a water depth of 15 m, between 11 and 40 minutes for a water depth of 20 m, and between 12 and 42 minutes for a water depth of 25 m. It can be hypothesized that this interesting difference is mainly caused by a two factors. Firstly, by the earlier mentioned fact that shallow water is inducive to the formation of a surface plume. All 15 m scenarios show the collection of sediment higher up in the plume after the first few minutes. This can be seen in the SSC cross-section graphs in Appendix D. This uplift of the plume prevents the sediment in all scenarios with a water depth of 15 m to reach the 20% in less than 21 minutes; in deeper water, much shorter plume ages are possible at 20% of the fines overflow flux (11 and 12 minutes). The second reason why the variation of plume ages at 20% of the overflow flux is relatively small, can be sought in the high end of the range. In 15m deep water, it takes at most 35 minutes before the fines flux has reduced to 20% of the overflow fines flux, whereas it can take 40 and 42 minutes respectively in 20 m and 25 m deep water under the conditions tested. The explanation for this can be sought in the shorter distance that the particles have to travel to the bed in 15 m deep water, as compared to deeper water.

- For low $\rho_{overflow}$ (1100 kg/m^3 and low u_{cf} (0.75 m/s), the plume age at 20% is highest for shallow water (15m), whereas for low $\rho_{overflow}$ (1100 kg/m^3) and high u_{cf} (1.5 m/s), the plume age is highest for deeper water (25 m).

Looking at Figure 4.3, it can be observed that, for a plume with a low overflow density (1100 kg/m^3) in shallow water (15m), u_{cf} hardly matters. The moment when the total fines flux as percentage of the overflow fines flux has decreased to 20% is reached at almost the same plume age for the three different values of u. In deep water, varying u has much more impact on the plume age at 20%: in 25 m deep water the 20% is reached much quicker when u_{cf} is low (0.75 m/s) than when u_{cf} is high (1.5 m/s). The combined effect of these things is so large, that the plume age at 20% is higher in shallow water for low u_{cf} and higher in deep water for high u_{cf} (the observation made in the bullet point). The explanation for all this can be found in the processes described earlier in this section. In shallow water, part of the plume is lifted up in the early stages of plume development, preventing the bulk of the particles to settle quickly. In deep(er) water, this effect is absent, leading to density-driven behavior if u_{cf} is low. If u_{cf} is high, the crossflow velocity will transport the particles further down the far-field where they will eventually settle, but because the shorter distance to the bottom, this will happen sooner in shallow water than in deep water.

- The difference in $\rho_{overflow}$ between 1200 kg/m^3 and 1300 kg/m^3 has little effect on the plume age at 20 %.

Looking at how long it takes before the total fines flux of the plume has decreased to 20% of the overflow fines flux, Figure 4.3 shows that there is little difference between the 1200 kg/m^3 and 1300 kg/m^3 scenarios. This can be explained by looking at the volume fractions of fines and sand in the overflow. These fractions are mentioned in the Chapter 3 and are repeated here for the convenience of the reader.

Volume fraction	*1100 kg/m3*	*1200 kg/m3*	*1300 kg/m3*
Fines	0.0432	0.0734	0.08
Sand	-	0.0315	0.086

Table 4.1: Composition overflow densities

Table 4.1 shows that the difference between the 1200 kg/m^3 and 1300 kg/m^3 overflows can mainly be attributed to the different volume fractions of sand. With regard to fines, the volume fractions in the two overflows are not that different. This can explain why the results of the corresponding runs were quite similar.

4.1.2. The magnitude of the sand plume

As discussed in the previous section, the plumes with the two larger overflow densities contain some sand. Figure 4.9 and Figure 4.10 show how the sand flux as percentage of the overflow sand flux developed over the first 60 minutes of the simulation runs. In the two figures, the results of six of the scenario runs are depicted. The results of the other runs lie in between the results pictured here. The figures show that the sand settled much quicker than the fines (for the results of the fines, see the previous section), and there are only small differences between the results of the various runs. In view of this, the results with regard to sand are not discussed further in this report.

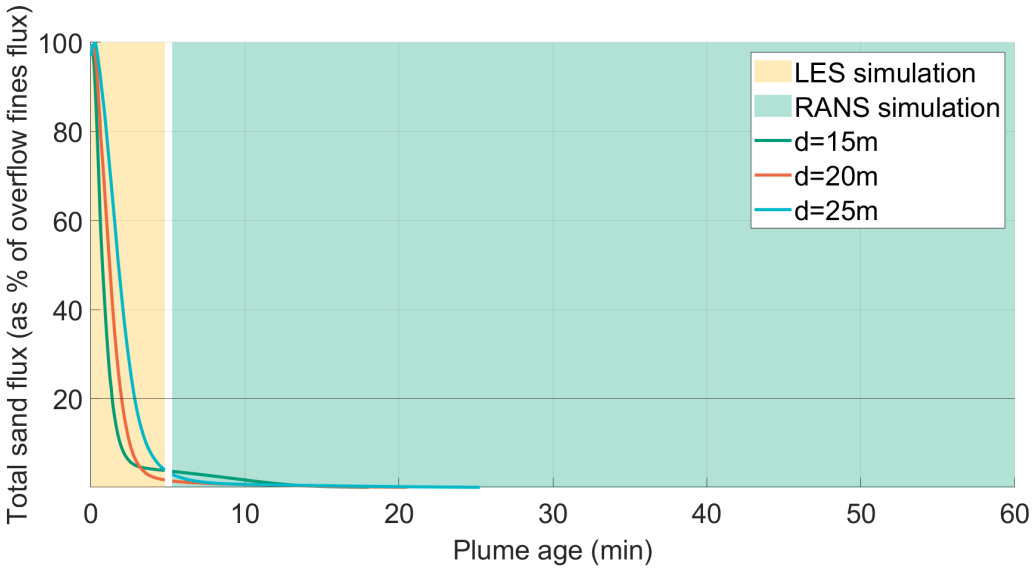

Figure 4.9: Sand flux (as % of overflow sand flux). For conditions: $\rho_{overflow} = 1200\ kg/m^3$ and $u_{cf} = 1.25\ m/s$

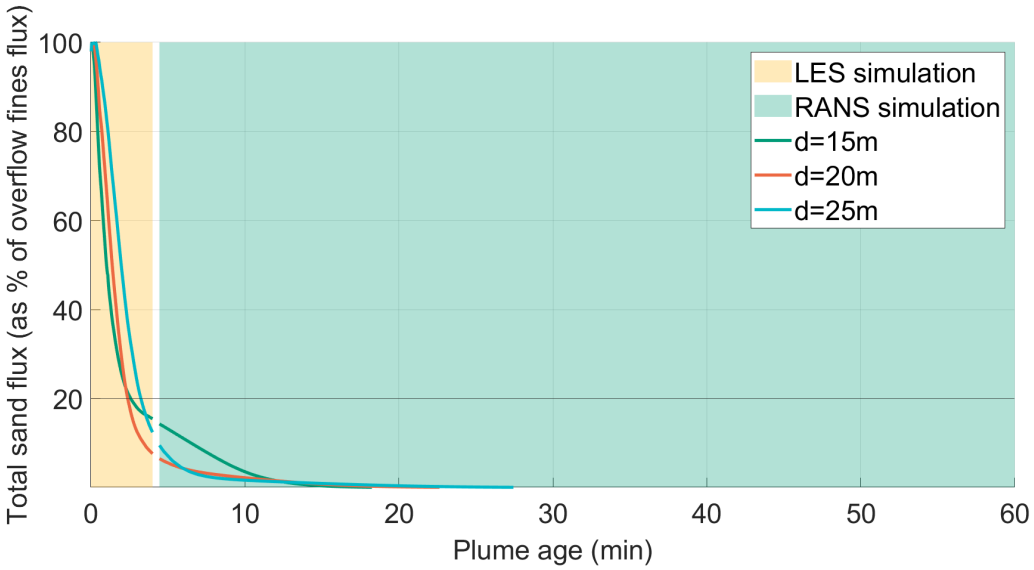

Figure 4.10: Sand flux (as % of overflow sand flux). For conditions: $\rho_{overflow} = 1200\ kg/m^3$ and $u_{cf} = 1.5\ m/s$

4.2. Vertical and lateral distribution of the plume

The previous section looked at the development of the total fines flux as percentage of the total overflow fines flux, particularly focusing on the moment when this percentage had decreased to 20%, because that percentage is often used in practice as source term for far-field models. The presented results were not solely related to this particular percentage, however: the % decrease of the fines overflow flux over the first 60 minutes of plume development was also looked at for a number of scenarios.

In addition to the development of the fines flux, the vertical distribution of the plume over the water column was also analyzed for a couple of the 27 scenarios, in order to better understand what is happening inside the plume, and connect this information to known processes discussed in Chapter 2.

This section takes a closer look at the vertical, and lateral, distribution of the fines in dredge plumes. Figures 4.11, 4.12, 4.13 and 4.14 show 3D images of the character of the plume at 7 different plume ages (1, 10, 20 30 40 50 and 60 minutes)for four of the 27 scenarios. These four scenarios were selected because they are a nice illustration of the extent to which the vertical and lateral distribution of the plume can differ, depending on the conditions.

The four figures depict cross-sections of the plume at the 7 plume ages chosen for this analysis. Besides the cross-sections, which show how the sediment is distributed horizontally and vertically, the corresponding total fines flux as percentage of the overflow fines flux is shown on the X-axis.

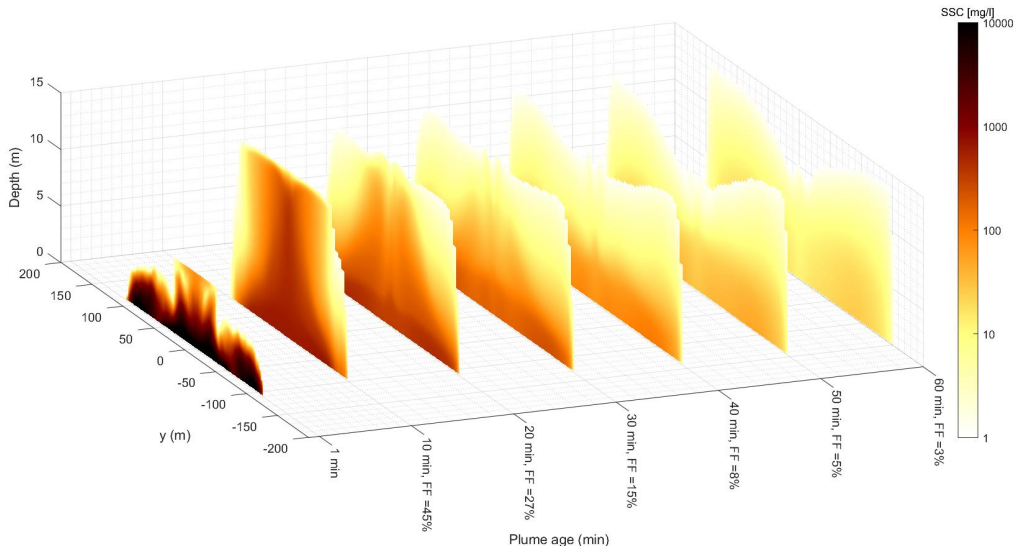

Figure 4.11: 3D Plume development up to 60 minutes. Conditions: $\rho_{overflow}$ = 1200 kg/m^3, d = 15 m, u_{cf} = 1.25 m/s (u_a = 0.5 m/s)

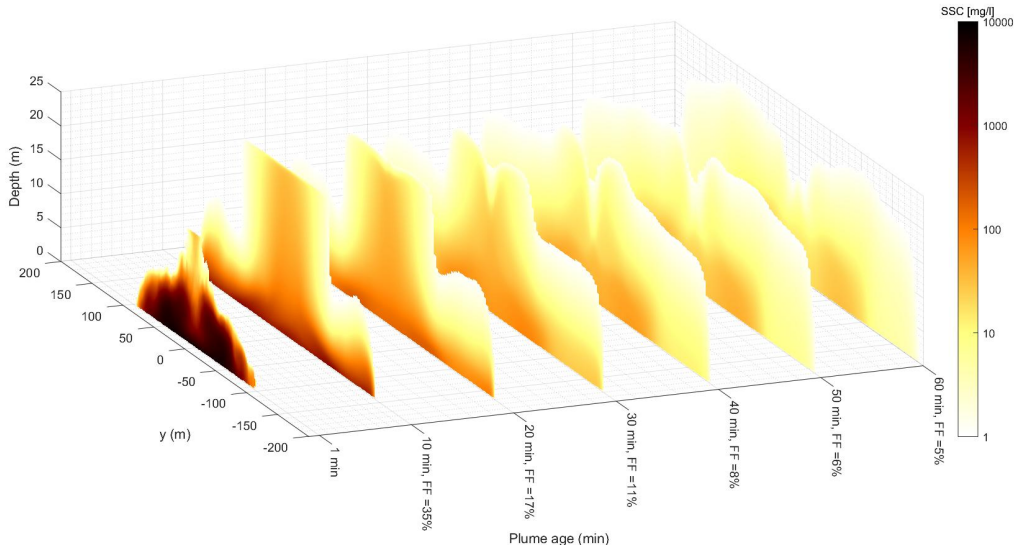

Figure 4.12: 3D Plume development up to 60 minutes. Conditions: $\rho_{overflow}$ = 1200 kg/m^3, d = 25 m, u_{cf} = 1.25 m/s (u_a = 0.5 m/s)

The conditions of the scenario depicted in Figure 1 are: an overflow density of 1200 kg/m^3, a crossflow velocity of 1.25 m/s and a water depth of 15 m. In the scenario depicted in Figure 4.12, only the water depth is different: 25 m. The first cross-section in the two pictures shows the character of the plume after one minute. Note that the plume does not reach to the top of the water column at this very early stage, because the dredging vessel takes up space in the top part of the water column. Most of the sediment can be found near the bottom. Looking at subsequent plume ages, at 10, 20, 30, 40, 50 and 60 minutes, we can see that the % of the fines overflow that is still in the plume continually decreases. This points to the (net) settling of sediment particles onto the bed. During this same time, the particles in the remaining part of the plume are continually being redistributed over the water column, both vertically and laterally. The plume gets wider and more diluted over time, and the contours get more rounded. Looking at the differences between Figures 4.11 and 4.12, we recognize the processes described in the previous section. Figure 4.11 shows that, in 15 m deep water, the plume is initially

mainly redistributed upwards. Figure 4.12 shows that, in 25 m deep water, the plume mainly spreads laterally across the bed, suggesting the formation of a pancake of sediment near the bed. Because the sediment stays close to the bottom, it can subsequently settle easily. Indeed, this appears to be the case: the fines flux in 25 deep water decreases more quickly in the first 40 minutes of plume development than the plume in 15 m deep water. Note that the laterally spreading (bed) plume in 25 m deep water ends up wider than the plume in the shallower water.

Let us now look at the character of the plume in two other scenarios, depicted in Figures 3 and 4. The water depth in the scenario of Figure 3 is 15 m, and in Figure 4 it is 25 m. The density of the overflow in these scenarios is again 1200 kg/m^3; the crossflow velocity is now 0.75 m/s. Be aware that the crossflow velocity is the combined effect of the ships velocity and the velocity of the ambient current. Since the velocity of the TSHD is 0.75 m/s in all scenarios, the velocity of the ambient current in these two scenarios is 0 m/s. This means that the development of the plume will take place at one location, namely the location of the dredging operation. There, at that one location, the plume will change character, and eventually settle.

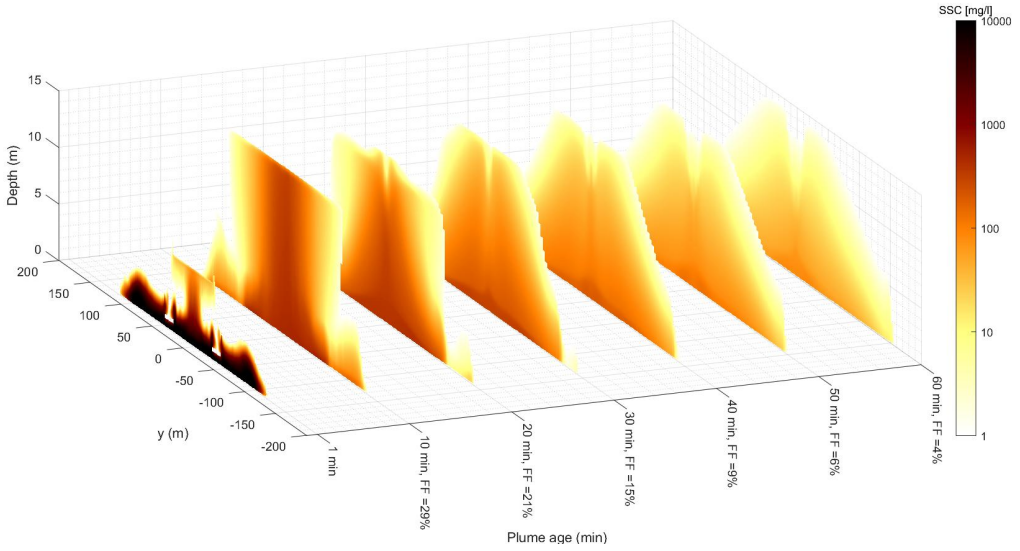

Figure 4.13: 3D Plume development up to 60 minutes. Conditions: $\rho_{overflow}$ = 1200 kg/m^3, d = 15 m, u_{cf} = 0.75 m/s (u_a = 0 m/s)

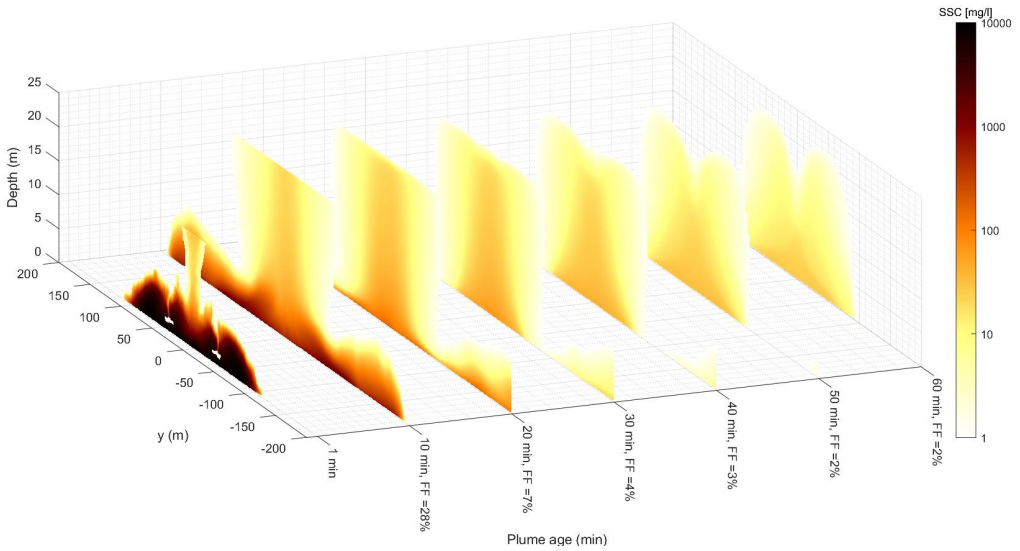

Figure 4.14: 3D Plume development up to 60 minutes. Conditions: $\rho_{overflow}$ = 1200 kg/m^3, d = 25 m, u_{cf} = 0.75 m/s (u_a = 0 m/s)

Comparing Figures 4.13 and 4.14 (crossflow velocity 0.75 m/s) with Figures 4.11 and 4.12 (crossflow velocity 1.25 m/s), we can observe that a lower crossflow velocity allows the plume to settle more quickly. The flux decreases at a faster rate, and there is more lateral spreading of the plume near the bed in Figures 4.13 and 4.14 than in Figures4.11 and 4.12. Comparing Figure 4.13 (15 m deep water) with Figure 4.14 (25 m deep water), we again see the effect of the water depth: in shallow water the plume is lifted upwards, and in deep water, the plume initially gets very wide across the bed. Interestingly, because much sediment is already deposited in the early stages of plume development in this scenario, the plume actually gets less wide from approximately 40 minutes onwards.

4.2.1. Lateral distribution: spreading

More information on the lateral distribution of the plume under various scenarios can be garnered from Figures 4.15, 4.16 and 4.17. Eagle eye views of three of the plumes are presented showing depth-averaged SSC values. The entire set is included in Appendix A.

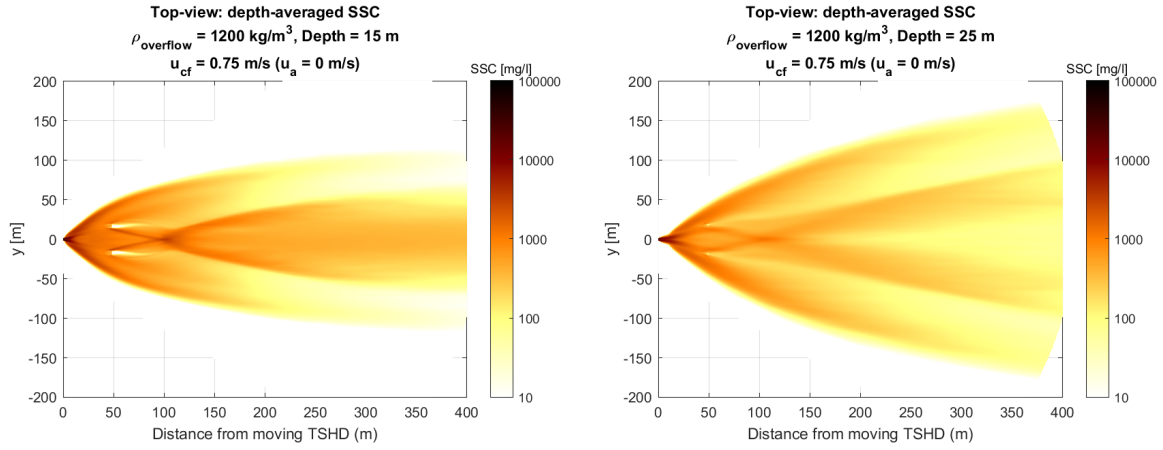

(a) d = 15 (m) **(b)** d = 25 (m)

Figure 4.15: Eagle-eye view of depth-averaged SSC. Conditions: 1200 kg/m^3, u_{cf} = 0.75 m/s

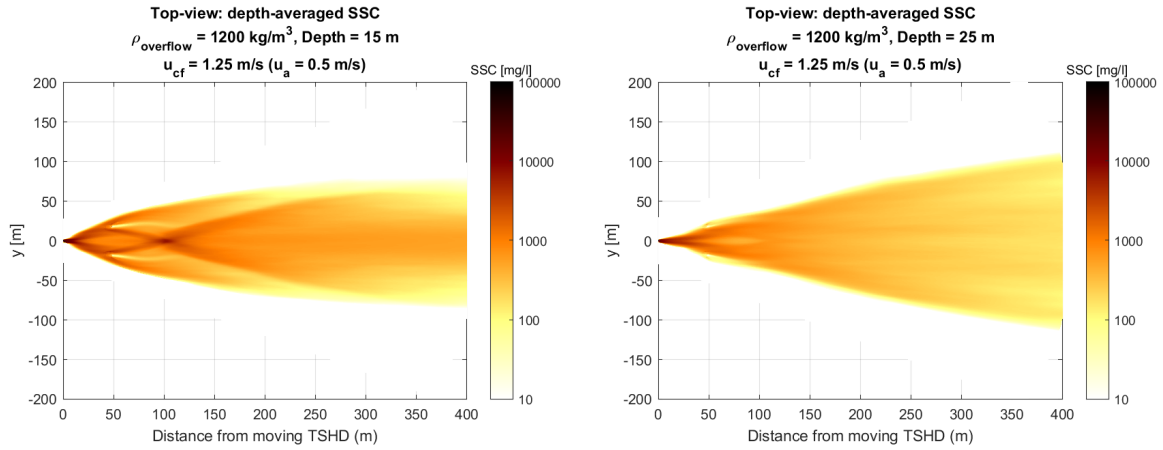

(a) d = 15 (m) **(b)** d = 25 (m)

Figure 4.16: Eagle-eye view of depth-averaged SSC. Conditions: 1200 kg/m^3, u_{cf} = 1.25 m/s

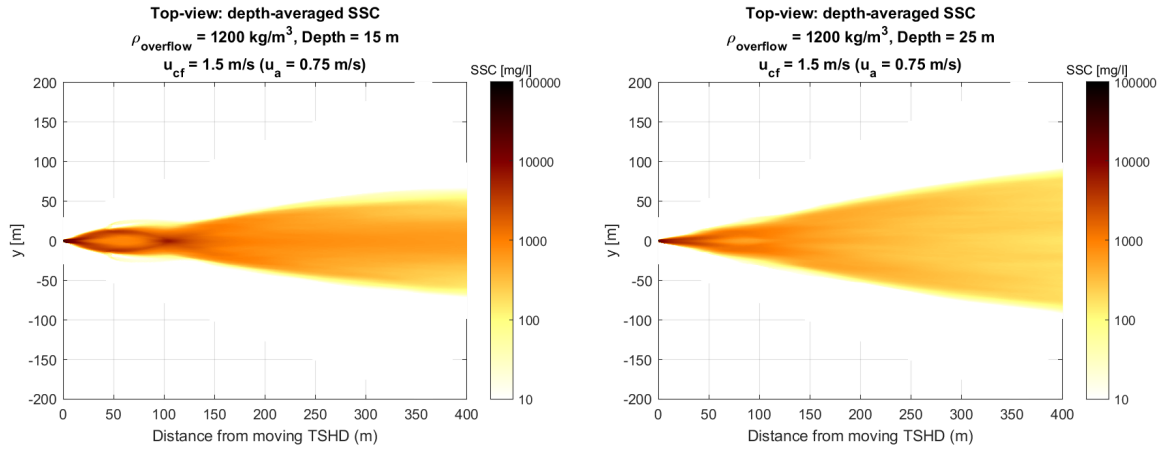

(a) d = 15 (m) **(b)** d = 25 (m)

Figure 4.17: Eagle-eye view of depth-averaged SSC. Conditions: 1200 kg/m^3, u_{cf} = 1.5 m/s

Looking at the figures, we can see the lateral width at the end of the 350 m, varies significantly.

A metric, the spreading angle, is introduced to express the rate of lateral spreading in the first 400 meters behind the vessel. From y = 0, at a distance of 400 m from the moving TSHD, the distance is found where the depth-averaged SSC reaches 10% of the depth-averaged centerline SSC. This is an arbitrary choice, but allows quick comparison between the plumes. The results are shown in Table 4.2.

d = 15 m	ρ_{of} = *1100 kg/m^3*	ρ_{of} = *1200 kg/m^3*	ρ_{of} = *1300 kg/m^3*
u_a = *0 m/s* + u_{tshd} = *0.75 m/s*	9	10	11
u_a = *0.5 m/s* + u_{tshd} = *0.75 m/s*	8	12	16
u_a = *0.75 m/s* + u_{tshd} = *0.75 m/s*	7	10	11

d = 20 m	ρ_{of} = *1100 kg/m^3*	ρ_{of} = *1200 kg/m^3*	ρ_{of} = *1300 kg/m^3*
u_a = *0 m/s* + u_{tshd} = *0.75 m/s*	14	24	25
u_a = *0.5 m/s* + u_{tshd} = *0.75 m/s*	10	15	19
u_a = *0.75 m/s* + u_{tshd} = *0.75 m/s*	7	11	14

d = 25 m	ρ_{of} = *1100 kg/m^3*	ρ_{of} = *1200 kg/m^3*	ρ_{of} = *1300 kg/m^3*
u_a = *0 m/s* + u_{tshd} = *0.75 m/s*	16	28	30
u_a = *0.5 m/s* + u_{tshd} = *0.75 m/s*	13	17	20
u_a = *0.75 m/s* + u_{tshd} = *0.75 m/s*	9	13	17

Table 4.2: Spreading angle in the first 400 m behind the moving TSHD under varying conditions

Table 4.2 confirms that conditions that contribute to a wide plume are high overflow density, deep water and a low crossflow velocity. This insight could be useful for predicting the area affected by the dredging operations under various circumstances.

4.2.2. Vertical distribution: contribution of the near-bed plume

Here, we take a closer look at the fines flux (as percentage of the total overflow fines flux) hovering in the bottom part of the water column, near the bed, over the first hour of plume development. We have already seen that this is a zone where the concentration of sediment can be high, as compared to the sediment in the higher parts of the water column. This is not surprising in itself, since the overflow starts out with downward momentum, is sent towards the bottom in a density-driven regime (under certain circumstances), and is subject to particle settling while the plume develops. Still, this phenomenon is worth a closer look, if only because it is an area that is difficult to measure in the field.

Figure 4.8, depicted in Section 4.1.1, showed how the % of overflow flux developed over the first 60 minutes, split up into the top and bottom part of the water column, for sediment with an overflow rho of 1200 kg/m^3 and a u of 0.75 m/s in scenarios with three different water depths. Here, we show a few other striking examples. Figure 4.18 represents a scenario with an overflow of low-density sediment in shallow water with a high cross flow velocity; Figure 4.19 represents a scenario with an overflow of high-density sediment in deep water with a low crossflow velocity.

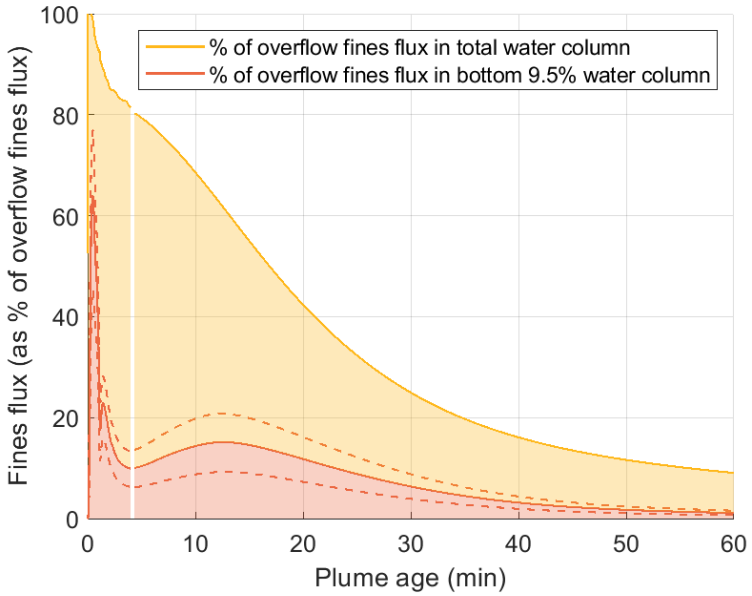

Figure 4.18: Fines flux (as % of overflow fines flux) in the total water column and the bottom 9.5 % of the water column.Conditions: $\rho_{overflow}$ = 1100 kg/m^3, d = 15 m, u_{cf} = 1.5 m/s (u_a = 0 m/s)

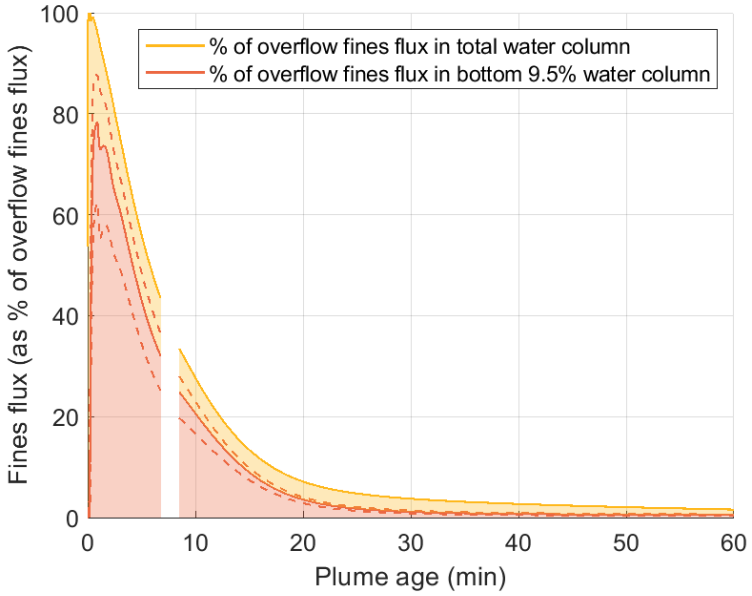

Figure 4.19: Fines flux (as % of overflow fines flux) in the total water column and the bottom 9.5 % of the water column.Conditions: $\rho_{overflow}$ = 1300 kg/m^3, d = 25 m, u_{cf} = 0.75 m/s (u_a = 0 m/s)

The reason for choosing 9.5% of the height of the water column as demarcation between the bottom and the top part of the water column, is the fact that field measurements are often carried out with an ADCP, and it is well known that ADCP measurements do not give accurate results in the bottom 6%-13% of the water column (see Chapter 2). This calls for using a different/additional method, in this case numerical simulation, to find out what is going on in this zone. For ease of interpretation, we have depicted a center line in the middle of the 6%-13% bandwidth at 9.5%. For the entire set of simulations, these figures are included in Appendix B.

Let us now look at Figures 4.18 and 4.19. In both scenarios, around 60% of the overflow flux ends up in the bottom part of the plume in the first one or two minutes. This happens immediately after the sediment has been ejected from the overflow shaft. After that, the two scenarios paint very different pictures. Depicting what happens under conditions of low-density sediment in shallow water with a high cross flow velocity, Figure C shows that in the next few minutes, approximately 20% of the overflow flux has disappeared. This means that this part of the plume has settled onto the bed. Interestingly, sizeable part of the remaining flux has at the same time moved from the near-bed zone to the top 92% of the water column. As hypothesized in the section where Figure 4.8 was discussed, several processes can play a role here: uplift of the plume in shallow water because of the influence of the propeller and/or sediment that is re-suspended after having settled, and is subsequently transported upwards in the midst of all the wild and chaotic movements of the plume and the ambient water around it. Approximately between minutes 4 and 10, some of the uplifted sediment sinks back to the near-bed zone, and this happens at a higher rate than the rate of sedimentation, hence the little bump we see in near-bed plume. After that, Figure 4.18 shows that the total fines flux steadily decreases until approximately 90% of the total fines have settled after one hour. All this time, most of the sediment is present in the top 92% of the water column.

Figure 4.19 looks very different. In this scenario - an overflow of high-density sediment in deep water with a low crossflow velocity we recognize a density-driven regime in the early stages, resulting in a sediment-laden zone near the bed from which there is no net upwards transport to the top 92% of the water column at any stage of plume development. The total fines flux as percentage of the total overflow fines flux decreases quickly, compared to the scenario depicted in Figure 4.18, which points to settling of the particles from the near-bed plume. This behavior can be explained by the combination of conditions

represented in this scenario. Firstly, the overflow sediment has a high density, which leads to a high Richardson number. In addition, the crossflow velocity is low, compared with the scenario depicted in Figure 4.18. This leads to a low velocity ratio. Like a high Richardson number, this indicates a density-driven regime. Figures 4.18 and 4.19 represent two scenarios which lead to large differences in plume development. Similar figures for the other 25 scenarios are included in this report as Appendix B.

4.3. Character plume at STF of 20 %

Implementing far-field source terms involves the determination of the magnitude of this source term, as well as the corresponding vertical and horizontal distribution of the suspended sediment in the plume, and the distance from the dredging source. Depending on the far-field model that is used, there are no hard and fast rules for choosing this location. In view of the current practice of using 20% of the overflow flux as source term fraction, we will now look at cross-sections of the simulation runs at the moment when the 20% is reached. (The results for the scenarios with an overflow density of 1300 kg/m^3 are not presented here, because they are very similar to those for 1200 kg/m^3. They can be found in Appendix C). For each cross-section, the corresponding distance from the dredging location and the plume age are also stated.

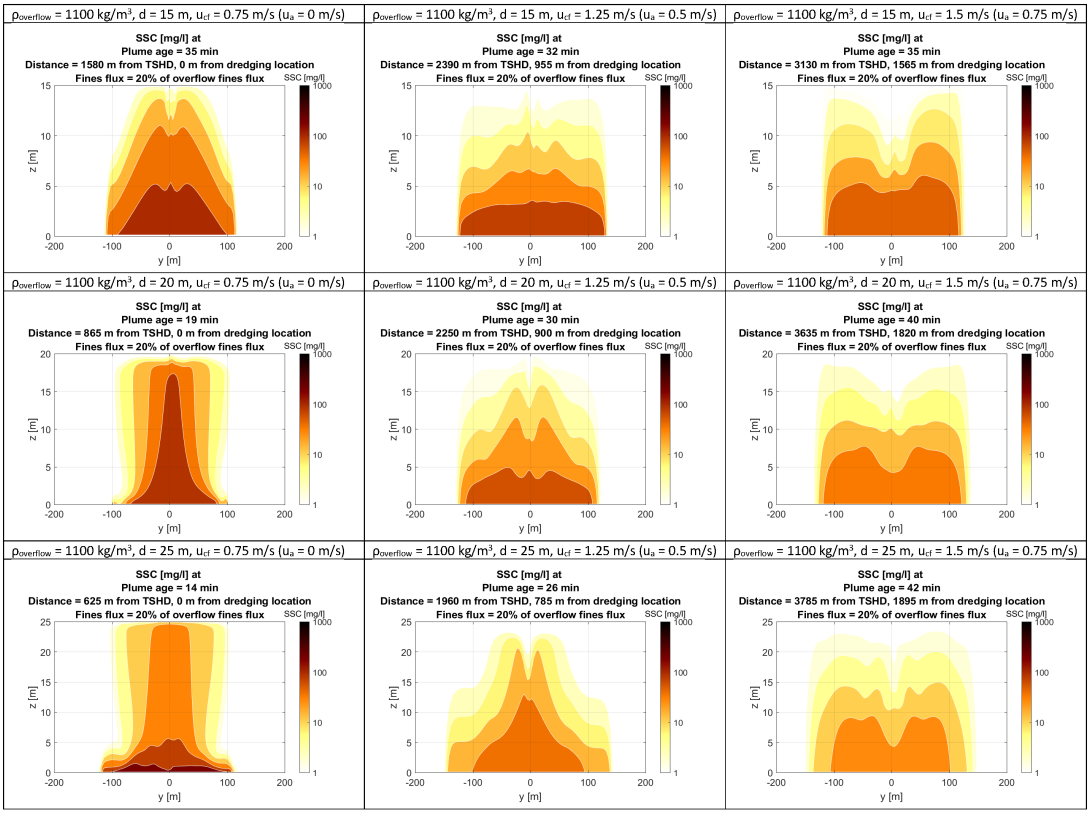

Figure 4.20: Character overflow plume when fines flux (as % of overflow fines flux) = 20 %.
Conditions: $\rho_{overflow} = 1100$

The cross-sections in Figure 4.20 reveal big differences between the cross-sections of the different scenarios. We will not go into the underlying processes here, since these have been discussed in the previous sections already. The cross-sections are presented here to stress the importance of (collecting and) incorporating knowledge about the lateral and vertical distribution of the plume when implementing the

far-field source term.

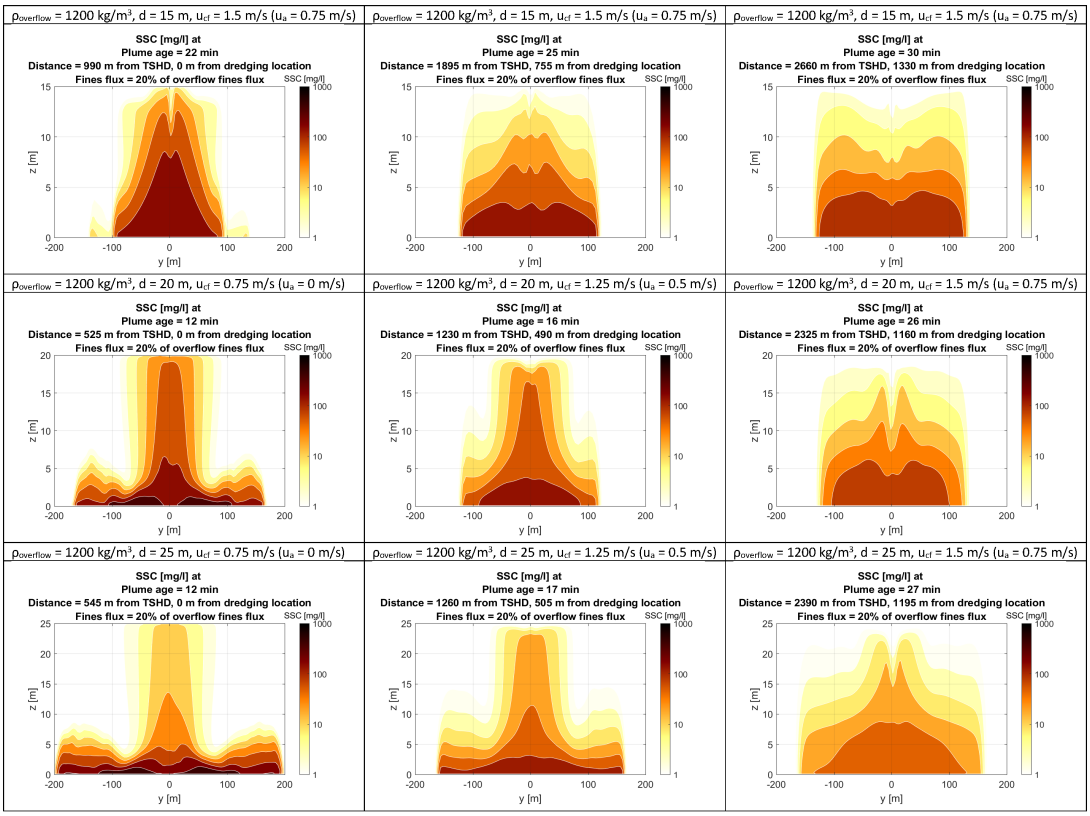

Figure 4.21: Character overflow plume when fines flux (as % of overflow fines flux) = 20 %. Conditions: $\rho_{overflow} = 1200$

5

Discussion

In this research the subject of estimating source terms for TSHD overflow plumes was investigated. This chapter starts off with a reflection on the research process as a whole in Section 6.1 In Section 6.2 a reflection of the results is given, focusing on the findings which were especially profound. Section 6.3 will elaborate on the contribution of this study by placing the results in perspective and revisiting key sources from literature. In the final section, Section 6.4, limitations and weaknesses of the research are identified and discussed.

5.1. Reflection on the research process

Even though a vast body of research exists on the development of dredge plumes and several guidelines exist for modelling these plumes, the topic is inherently complex and warranting further research. Although the general topic of this thesis was clear from the beginning, identifying an unambiguous knowledge gap with a fitting and feasible methodology turned out to be a difficult task.

A central question from the start was the area applicability of the reasonable range as presented by Becker et al. (2015) for the STF of a TSHD overflow plume. This method is widely used in the dredging industry in different stages of a dredging operation for a multitude of reasons. However, placing the STF concept at the center of the research proved to be tough. The authors do not clearly define where (at what distance from the dredging activity) the reasonable range of 0-20% is found. Following their definition for a STF, the 0-20% should be implemented at the transition from the near field to the far field. However, these zones are not sharply defined. Aside from the Local Plume Richardson number as presented by De Wit (2010), which proved difficult to apply, there are no robust metrics for this transition presented in the literature.

Another complicating factor regarding this transition, is the fact that any physics-based metric that is indicating the 'start' of the far-field does not necessarily coincide with the 'start' of a far-field model. Depending on modelling choices such as grid resolution, number of dimensions and included processes, a far-field model will be able to represent more or less dynamic behavior (e.g., density driven behavior, turbulence). Ultimately, it is up to the modeller to make such modelling choices and to make informed choices regarding source term implementation on the far-field computational grid. What we see in practice is that the STF of 0-20% is often implemented at the location of dredging activity. This current practice deviates from the intended use of STF concept.

As a result of the challenges mentioned above, making unequivocal statements on the conditions where the STF concept is applicable (or not) proved to be unworkable. Coming across these challenges, the

research evolved. Instead of clear-cut refinement of the $0-20\%$ range, this research presents conclusions which aid the dredging industry to implement source terms in a more informed way.

5.2. Reflection on the results

The results clearly show the significant contribution of the sediment in the bottom 6-13 % of the water column to the total amount of sediment in the water column. What happens in this bottom 6-13% is specifically interesting because it represents the part of the water column that is typically missed by the ADCP. One could argue that, when interested in SSC in the far-field, what happens in this zone is not that relevant because the sediment in that zone is prone to quick settling. But, perhaps it does: the results show that, under certain conditions, this sediment is largely re-entrained out of the bed plume into the ambient water above, before settling eventually. ADCP measurements close to the vessel might therefore give a wrong impression that most of the sediment has settled.

In general, the results of this study are in line with, and build upon, existing work. The results confirm findings by Decrop and Sas (2018) about the contributing effect of a low overflow density on the generation of a surface plume. De Wit et al. (2022) also used CFD modelling to study STF magnitudes in overflow plumes and made a comparison with the STF-concept. At plume ages of 30 and 60 minutes, the authors found fines fluxes comparable to the Becker STF. These plume ages are higher than the ones in this study (11-42 min), but the two studies differ on various aspects so cannot be compared in a straightforward manner. One contributing factor could be the higher floc settling velocities in this study (roughly three times as high).

5.3. Contributions of this study

The results of this study contribute in a number of ways to the existing body of research. To start with, the TUDflow3D simulation runs have shown that TSHD dredge plume fluxes can still be significant a few hundred meters from the overflow, an area commonly believed to mark the transition between the near-field and the far-field where the flux is believed to have decreased to 0-20% of the overflow flux. This study has shown that this fraction can be much higher at that distance under given conditions. This is relevant because it may indicate that the plume still shows (some) dynamic behavior. Field measurements at the start of a project are definitely warranted to arrive at correct source terms. It should be noted that this was also stressed by Becker et al. (2015). For cases where such measurements are not feasible, the results of this study gives some guidance on where to implement the 0-20% source term fraction under various circumstances. Or, if an implementation closer to the vessel is desired, it gives guidance on which (higher) source term fraction is appropriate.

A second contribution of this study lies in using a well-respected numerical model to produce extensive simulation results on the vertical and horizontal distribution of the dredge plume, under various conditions and over time. This information gives a deeper insight into what happens inside of the dredge plume, showing where in the water column the sediment is situated and how this distribution changes over time. Combining this information with theoretic background information sheds light on how the various hydrodynamic processes form the plume. As Tuinhof (2014) has shown, knowledge about the horizontal and vertical distribution of the plume is important for obtaining reliable predictions of SSC in the far-field. The results of this study confirm this. Both the horizontal and vertical distribution of suspended sediment is skewed and changes as the plume develops. The distribution also varies with the conditions tested. This information should be incorporated in the implementation of the source term. This improves the quality of far-field SSC predictions, since implementation of the source term involves making assumptions/choices about the distribution of sediment.

A third contribution is the insight this study offers into the effects of three relevant conditions on plume

formation and development: the crossflow velocity, the density of the sediment and the water depth. Although the effect of these conditions is generally known from other studies, this thesis gives more insight into why these effects take place, for example by linking the plumes flux development under the studied conditions to the distribution of the sediment in the plume. The research also has practical relevance. The findings about the effects of various crossflow velocities on the magnitude of the flux, for example, are of direct use to dredging companies about to start a dredging project. They can use the results of this simulation study and combine it with knowledge of the local conditions to produce estimations of the expected plume that are as realistic as possible.

5.4. Limitations of this study

The main limitations of this research have to do with the assumptions and simplifications made for running the model. Some important assumptions are listed below.

- *Soil conditions.* In practice, many different soil types are dredged: this research limits itself to mud-sand mixtures. The particle size distribution (PSD) of the sediment, is represented by only two sediment fractions, whereas in reality a PSD consists of many more.
- *Settling velocities* Assumptions are made with regard to the settling velocity of the sediment and the degree of flocculation, etc. In the numerical simulation, 3.5 mm/s is used as settling velocity of the fines. Using 1 mm/s, also a realistic value, would lead to lower deposition and longer times before the 0-20% range of Becker et al. (2015) is reached.
- *Idealized conditions* The model conditions - apart from the varied conditions - are idealized: the sailing speed, ambient current and sailing direction are all constant in time for the duration of the simulation. In reality, dredging operations often take place in conditions with varying current speeds and currents coming from various directions.

Obviously, making assumptions and simplifications is inherent to using a model, but it is important to be aware of, since it adds an unknown amount of uncertainty to the results. When TUDflow3D (or another numerical model) is used to estimate dredge plumes in a real-life project, care should be taken to make all model inputs reflect the local circumstances as much as possible.

6

Conclusions and Recommendations

6.1. Conclusions

The objective of this study was to support a more informed implementation of TSHD source terms on the far-field computational grid. This aim translated into three research questions, which are repeated here for the convenience of the reader. Per question, the conclusions are presented.

- The first research question was: *'At which plume age and distance from the overflow shaft is the 0-20% range for the overflow source term fraction, as introduced by Becker et al. (2015), found under various conditions?*

This research has shown that the 20% STF (when considering the plume flux over the entire water column) can be found at a wide range of plume ages (and distances). Across the scenarios studied in this research, this ranged from 11-42 minutes in plume age and 0-1895 m in distance from the dredging location (515-3785 m from the moving TSHD).

The simulation runs for the various combinations of conditions (a water depth of 15, 20 or 25 meter, a crossflow velocity of 0.75, 1.25 or 1.5 m/s and an overflow density of 1100, 1200 or 1300 kg/m^3) have shown that the total sediment flux decreases fastest when the water is deep, the crossflow velocity is low and the overflow density is high. These conditions lead to strong density-driven behavior. Table 6.1 shows the distance from the dredging location where the 20% STF is found, for each individual simulation.

d = 15 m	ρ_{of} = *1100 kg/m^3*	ρ_{of} = *1200 kg/m^3*	ρ_{of} = *1300 kg/m^3*
u_a = *0 m/s* + u_{tshd} = *0.75 m/s*	0	0	0
u_a = *0.5 m/s* + u_{tshd} = *0.75 m/s*	955	755	730
u_a = *0.75 m/s* + u_{tshd} = *0.75 m/s*	1565	1330	1270

d = 20 m	ρ_{of} = *1100 kg/m^3*	ρ_{of} = *1200 kg/m^3*	ρ_{of} = *1300 kg/m^3*
u_a = *0 m/s* + u_{tshd} = *0.75 m/s*	0	0	0
u_a = *0.5 m/s* + u_{tshd} = *0.75 m/s*	900	490	510
u_a = *0.75 m/s* + u_{tshd} = *0.75 m/s*	1815	1160	1155

d = 25 m	ρ_{of} *= 1100 kg/m^3*	ρ_{of} *= 1200 kg/m^3*	ρ_{of} *= 1300 kg/m^3*
u_a *= 0 m/s +* u_{tshd} *= 0.75 m/s*	0	0	0
u_a *= 0.5 m/s +* u_{tshd} *= 0.75 m/s*	785	500	515
u_a *= 0.75 m/s +* u_{tshd} *= 0.75 m/s*	1895	1195	1170

Table 6.1: Distance from dredging location where total fines flux = 20% of overflow fines flux

When the 20% STF is implemented at the dredging location, which is common, the data in Table 6.1 also represent the error that is made in meters.

- The second research question was: *Under various conditions, what is the character of the vertical and lateral distribution of the TSHD dredge plume?*

Both the vertical and the lateral distribution of the plume change over time as the plume develops, and are influenced by the conditions varied in this study: the water depth, the overflow density and the ambient current velocity. In the first few minutes after leaving the TSHD overflow, a large fraction of the plume ends up in the bottom 6-13% of the water column. In conditions of deep water, a high overflow density and a low crossflow velocity, this remains the case in the first 60 minutes of plume age. This means that the turbidity will disappear relatively quickly and occurs mainly in the bottom zone of the water column under these circumstances; density-driven behavior dominates the development of the plume. This conclusion is in line with the conclusion of the first research question, about the rate with which the sediment flux diminishes under various circumstances, underlining the connection between the way the sediment is distributed over the water column and the fate of the plume as a whole.

With regard to the lateral distribution of the plume, the effects of several key processes in plume development can be recognized in the simulation results. Four minutes after leaving the overflow shaft, SSC cross-sections clearly show the dynamic behavior of the plume. It can be seen that the large fraction of sediment present in the bottom part of the water column, mentioned above, has impinged on the seabed and is forming a laterally spreading bed plume. In this early stage of plume development, the formation of a surface plume can also be seen. Conditions that are conducive to surface plume formation are shallow water, low density sediment. After the initial stage, the suspended sediment spreads laterally and gradually settles onto the bed.

Conditions that contribute to a laterally spreading (bed)plume are: deep water, a low cross-flow velocity and high overflow density.

- The third research question was: *How can current practice regarding the implementation of source terms be improved?*

In practice, source terms are often implemented as a virtual source at the location of dredging activity. This is also common practice for the 20% STF as presented by Becker et al. (2015). Assessing Table 6.1 and the variety of the vertical and lateral distributions, we can conclude that this approach is too blunt an instrument to do justice to the complex character of TSHD dredge plumes. The current practice can be improved by making more informed modelling choices to (1) account for the non-uniformity and skewed distribution of the source term and (2) to take into account the local conditions. Scenarios with conditions where density-driven behavior is present for a longer period might require more advanced far-field models.

Concrete recommendations with regard to implementing source terms are proposed in the next section.

6.2. Recommendations

The remainder of this section discusses a number of recommendations that can be made on the basis of this study. These recommendations are aimed at obtaining a more complete picture of the environmental impact of dredging activities.

6.2.1. Recommendations for the dredging industry

- When implementing source term fractions in a far-field model, avoid implementing them as a virtual source at the location of dredging, since this could lead to a sizeable underestimation of the magnitude of the plume.

- When possible, complement the use of the STF concept with the use of a near-field model such as TUDflow3D. Even by simulating the first 5 minutes of plume development, the implementation of STs in a far-field model will be more informed.

- If measurements or the use of a near-field model are not feasible, seek guidance from the results of this study (e.g. Table 6.1) to obtain a first indication of the adjustments to the source term fraction necessary to reflect local conditions.

6.2.2. Recommendations for future research

- Quantify the underestimation of the source term that results from implementing STFs at the location of dredging activity. The validated CFD model TUDflow3D could be brought in to quantify the extent of this underestimation in terms of SSC and/or flux.

- The second recommendation regards model coupling; even when the exact character and magnitude of the plume are known when entering a far-field model, the far-field results will be inaccurate if the model is not able to capture the processes governing plume development. For a modeller to be able to know whether or not their far-field model has a sufficient resolution, a physics-based metric for the 'transition' can still be useful. TUDflow3D has the unique capacity to capture the complex mix of processes. The model output thus forms a rich dataset, containing velocities, densities and concentrations.

- Flocculation parameters have a relatively large impact on model ouput: larger floc diameters result in greater settling velocities and therefore a more rapid decrease in fines flux and SSC. There is a lack of knowledge on the topic in general, but particularly on the role it plays in dredge plume development: it is poorly understood what degree of flocculation takes place at different stages during the dredging cycle. Insight can be gained on this topic by performing field measurements with instruments such as a LISST, which are able to measure in-situ particle size distributions. Adding to the current body of data of floc diameters, in-situ PSDs, allows for more informed choices with regard to flocculation parameters.

References

Aarninkhof, S. G., Rosenbrand, W., van Rhee, C., & Burt, T. (2008). The day after we stop dredging: A world without sediment plumes? *Terra et Aqua*, *110*, 15.

Adnitt, C., & Van Koningsveld, M. (2018). Assessment and management of sustainability. In P. Laboyrie, M. van Koningsveld, S. Aarninkhof, C. Fletcher, & T. van Dam (Eds.), *Dredging for sustainable infrastructure*. CEDA/IADC.

Ardalan, H., & Vafaei, F. (2019). Cfd and experimental study of 45ř inclined thermal-saline reversible buoyant jets in stationary ambient. *Environmental Processes*, *6*(1), 219–239. https://doi.org/10.1007/s40710-019-00356-z

Becker, Van Eekelen, E., Wiechen, V., de Lange, Damsma, T., Smolders, T., & Van Koningsveld, M. (2015). Estimating source terms for far field dredge plume modelling. *Journal of Environmental Management*, *149*, 282–293. https://doi.org/https://doi.org/10.1016/j.jenvman.2014.10.022

Bridges, T., & Vellinga, T. (2018). Integrating dredging in sustainable development. In P. Laboyrie, M. van Koningsveld, S. Aarninkhof, C. Fletcher, & T. van Dam (Eds.), *Dredging for sustainable infrastructure*. CEDA/IADC.

Castro, B., Mestemaker, B., & van den Heuvel, H. (2019). Towards zero emission work vessels: The case of a dredging vessel. *Proceedings of International Conference on Modelling and Optimisation of Ship Energy Systems*.

Chen, Q.-y., He, Y.-p., Xiong, T., Li, M.-z., & Liu, W.-h. (2022). Study on the dynamic characteristics of the overflow advection and diffusion of trailing suction hopper dredgers based on cfd. *Ocean Engineering*, *252*, 111263.

Cintolesi, C., Petronio, A., & Armenio, V. (2019). Turbulent structures of buoyant jet in cross-flow studied through large-eddy simulation. *Environmental Fluid Mechanics*, *19*(2), 401–433. https://doi.org/10.1007/s10652-018-9629-1

Cunning, R., Silverstein, R. N., Barnes, B. B., & Baker, A. C. (2019). Extensive coral mortality and critical habitat loss following dredging and their association with remotely-sensed sediment plumes. *Marine Pollution Bulletin*, *145*, 185–199.

Dai, C., Jia, L., Zhang, J., Shu, Z., & Mi, J. (2016). On the flow structure of an inclined jet in crossflow at low velocity ratios. *International Journal of Heat and Fluid Flow*, *58*, 11–18. https://doi.org/10.1016/j.ijheatfluidflow.2015.12.001

De Wit, L. (2010). Near field 3d cfd modelling of overflow plumes. *Proceedings of WODCON XIX, Beijing, China*.

De Wit, L. (2015). *3d cfd modelling of overflow dredging plumes* (Doctoral dissertation). Technische Universiteit Delft.

De Wit, L., Bliek, B., & Rhee, C. V. (2020). Can surface turbidity plume generation near a trailing suction hopper dredger be predicted? *Terra et Aqua*.

De Wit, L., van Rhee, C., & Talmon, A. (2014). Influence of important near field processes on the source term of suspended sediments from a dredging plume caused by a trailing suction hopper dredger: The effect of dredging speed, propeller, overflow location and pulsing. *Environmental Fluid Mechanics*, *15*, 41–66.

De Wit, L., Van Weerdenburg, R., Van Der Biezen, T., & Mosca, C. (2022). 3d cfd modelling of barge filling and overflow dredging plume to determine the far-field source term. *WODCON XXIII*.

Decrop, B., Sas, M., Mulder, T. D., & Toorman, E. (2018). Large-eddy simulations of a sediment plume released by a dredger using overflow. *Journal of Applied Water Engineering and Research*, *6*(1), 62–69. https://doi.org/10.1080/23249676.2016.1209441

Decrop, B., & Sas, M. (2018). Towards improved prediction of dredging plumes : Numerical and physical modelling by.

Erftemeijer, P. L., Riegl, B., Hoeksema, B. W., & Todd, P. A. (2012). Environmental impacts of dredging and other sediment disturbances on corals: A review. *Marine Pollution Bulletin*, *64*(9), 1737–1765. https://doi.org/https://doi.org/10.1016/j.marpolbul.2012.05.008

Fischer, H., List, E., Koh, R., Imberger, J., & Brooks, N. (1979). Chapter 9 - turbulent jets and plumes. In H.B.Fischer, E. List, R. Koh, J.Imberger, & N. Brooks (Eds.), *Mixing in inland and coastal waters* (pp. 315–389). Academic Press. https://doi.org/https://doi.org/10.1016/B978-0-08-051177-1.50013-1

IADC. (2010). *Dredging for development* (tech. rep.).

IADC. (2020a). *Dredging in figures* (tech. rep.).

IADC. (2020b). *Facts about dredging plant and equipment,* (tech. rep.).

Kemps, H., & Masini, R. (2017). *Estimating dredge source terms–a review of contemporary practice in the context of environmental impact assessment in western australia* (tech. rep.).

Laboyrie, P., van Koningsveld, M., Aarninkhof, S., Fletcher, C., & van Dam, T. (Eds.). (2018). *Dredging for sustainable infrastructure*. CEDA/IADC.

Lisi, I., Feola, A., Bruschi, A., Pedroncini, A., Pasquali, D., & Di Risio, M. (2019). Mathematical modeling framework of physical effects induced by sediments handling operations in marine and coastal areas. *Journal of Marine Science and Engineering*, *7*(5), 149.

Miedema, S., & Becker, S. (1993). The use of modelling and simulation in the dredging industry in particular the closing process of clamshell dredges. *In proceedings: CEDA Dredging Days*.

Mikkelsen, O., & Pejrup, M. (2001). The use of a lisst-100 laser particle sizer for in-situ estimates of floc size, density and settling velocity. *Geo-Marine Letters*, *20*, 187–195. https://doi.org/10.1007/s003670100064

Mueller, D. S., Wagner, C. R., & Winkler, M. F. (2007). Best practices for measuring discharge with acoustic doppler current profilers.

Saremi, S. (2014). *Density-driven currents and deposition of fine materials* (Doctoral dissertation). Technical University of Denmark.

Smith, S., & Friedrichs, C. (2011). Size and settling velocities of cohesive flocs and suspended sediment aggregates in a trailing suction hopper dredge plume. *Continental Shelf Research - CONT SHELF RES*, *31*. https://doi.org/10.1016/j.csr.2010.04.002

Spearman, J., Bray, R., Land, J., Burt, T., Mead, C., & Scott, D. (2007). Plume dispersion modeling using dynamic representation of trailer dredger source terms. *Proceedings in Marine Science*, *8*. https://doi.org/10.1016/S1568-2692(07)80025-8

Spearman, Taylor, J., Crossouard, N., Cooper, A., Turnbull, M., Manning, A., Lee, M., & Murton, B. (2020). Measurement and modelling of deep sea sediment plumes and implications for deep sea mining. *Scientific Reports*, *10*(1), 5075. https://doi.org/10.1038/s41598-020-61837-y

Stewart, J. P., & Leaman, C. K. (2013). Validation of dredge plume modelling inputs. *Coasts and Ports 2013: 21st Australasian Coastal and Ocean Engineering Conference and the 14th Australasian Port and Harbour Conference*, 715–720.

Sun, C., Branson, P., & Mills, D. (2020). *Guideline on dredge plume modelling for environmental impact assessment* (tech. rep.). Western Australian Marine Science Institution.

Sun, C., Shimizu, K., & Symonds, G. (2016). Numerical modelling of dredge plumes: A review. *Report of Theme*, *45*.

Taherian, M., & Mohammadian, A. (2021). Buoyant jets in cross-flows: Review, developments, and applications. *Journal of Marine Science and Engineering*, *9*, 61. https://doi.org/10.3390/jmse9010061

Todd, V. L. G., Todd, I. B., Gardiner, J. C., Morrin, E. C. N., MacPherson, N. A., DiMarzio, N. A., & Thomsen, F. (2014). A review of impacts of marine dredging activities on marine mammals. *ICES Journal of Marine Science*, *72*(2), 328–340. https://doi.org/10.1093/icesjms/fsu187

Tohidi, A., & Kaye, N. (2016). Highly buoyant bent-over plumes in a boundary layer. *Atmospheric Environment*, *131*, 97–114. https://doi.org/10.1016/j.atmosenv.2016.01.046

Tuinhof, T. (2014). *Modelling far-field dredge plume dispersion* (Master's thesis). Delft University of Technology.

United Nations. (2015). *Transforming our world: The 2030 agenda for sustainable development* (Agenda A/RES/70/1). United Nations. New York. https://sdgs.un.org/2030agenda

Van Eekelen, E. (2007). *Experimental research on dynamic dredge overflow plumes* (Master's thesis). Delft University of Technology.

Van Prooijen, B. C., & Winterwerp, J. C. (2010). A stochastic formulation for erosion of cohesive sediments. *Journal of Geophysical Research: Oceans*, *115*(C1). https://doi.org/https://doi.org/10.1029/2008JC005189

Van Raalte, G., & Parys, M. (2018). Equipment and methods. In P. Laboyrie, M. van Koningsveld, S. Aarninkhof, C. Fletcher, & T. van Dam (Eds.), *Dredging for sustainable infrastructure*. CEDA/IADC.

van Eekelen, E., Wiechen, J., & van Koningsveld, M. (2015). Practical use of dredge plume source terms.

Vikolainen, V., Bressers, H., & Lulofs, K. (2014). A shift toward building with nature in the dredging and port development industries: Managerial implications for projects in or near natura 2000 areas. *Environmental Management*, *54*. https://doi.org/10.1007/s00267-014-0285-z

Wang, X., & Mohammadian, A. (2022). Numerical simulations of 15-degree inclined dense jets in stagnate water over a sloped bottom [Cited by: 0]. *Lecture Notes in Civil Engineering*, *240*, 63–74. https://doi.org/10.1007/978-981-19-0507-0_7

Wasim, J., & Nine, A. H. J. (2017). Challenges in developing a sustainable dredging strategy [10th International Conference on Marine Technology, MARTEC 2016]. *Procedia Engineering*, *194*, 394–400. https://doi.org/https://doi.org/10.1016/j.proeng.2017.08.162

Wenger, A. S., Harvey, E., Wilson, S., Rawson, C., Newman, S. J., Clarke, D., Saunders, B. J., Browne, N., Travers, M. J., Mcilwain, J. L., et al. (2017). A critical analysis of the direct effects of dredging on fish. *Fish and Fisheries*, *18*(5), 967–985.

Winterwerp, J. C. (2002). Near-field behavior of dredging spill in shallow water. *Journal of Waterway, Port, Coastal, and Ocean Engineering*, *128*(2), 96–98. https://doi.org/10.1061/(ASCE)0733-950X(2002)128:2(96)

World Commission on Environment and Development. (1987). *Our common future* (tech. rep.). Oxford University Press.

Zhao, S., Yang, Z., Zhang, Q., Sun, J., & Wang, Y. (2018). Experimental study on temperature spread of multi-angle inclined buoyant jet. *Proceedings of IOP Conference Series: Earth and Environmental Science*, *191*(1). https://doi.org/10.1088/1755-1315/191/1/012063

natbib

A

Spreading angle

...

Figure A.1: Spreading of depth-averaged SSC for the first 350 meters of plume development (from moving vessel). Nine simulations with overflow density = 1100 kg/m^3

Figure A.2: Spreading of depth-averaged SSC for the first 350 meters of plume development (from moving vessel). Nine simulations with overflow density = 1200 kg/m^3

Figure A.3: Spreading of depth-averaged SSC for the first 350 meters of plume development (from moving vessel). Nine simulations with overflow density = 1300 kg/m^3

B

Vertical distribution: contribution of the bottom of the water column

...

Figure B.1: Fines flux as % of overflow fines flux. Red shaded area represents the amount of sediment in the bottom 9.5% of the water column. Nine simulations with overflow density of 1100 kg/m^3

Figure B.2: Fines flux as % of overflow fines flux. Red shaded area represents the amount of sediment in the bottom 9.5% of the water column. Nine simulations with overflow density of 1200 kg/m^3

Figure B.3: Fines flux as % of overflow fines flux. Red shaded area represents the amount of sediment in the bottom 9.5% of the water column. Nine simulations with overflow density of 1300 kg/m^3

C

SSC Cross-sections: at fines flux = 20% of overflow fines flux

...

Figure C.1: SSC cross-sections plume where fines flux = 20% of overflow flux. Nine simulations with overflow density of 1100 kg/m^3

Figure C.2: SSC cross-sections plume where fines flux = 20% of overflow flux. Nine simulations with overflow density of 1200 kg/m^3

Figure C.3: SSC cross-sections plume where fines flux = 20% of overflow flux. Nine simulations with overflow density of 1300 kg/m^3

D

SSC Cross-sections: 60 minutes

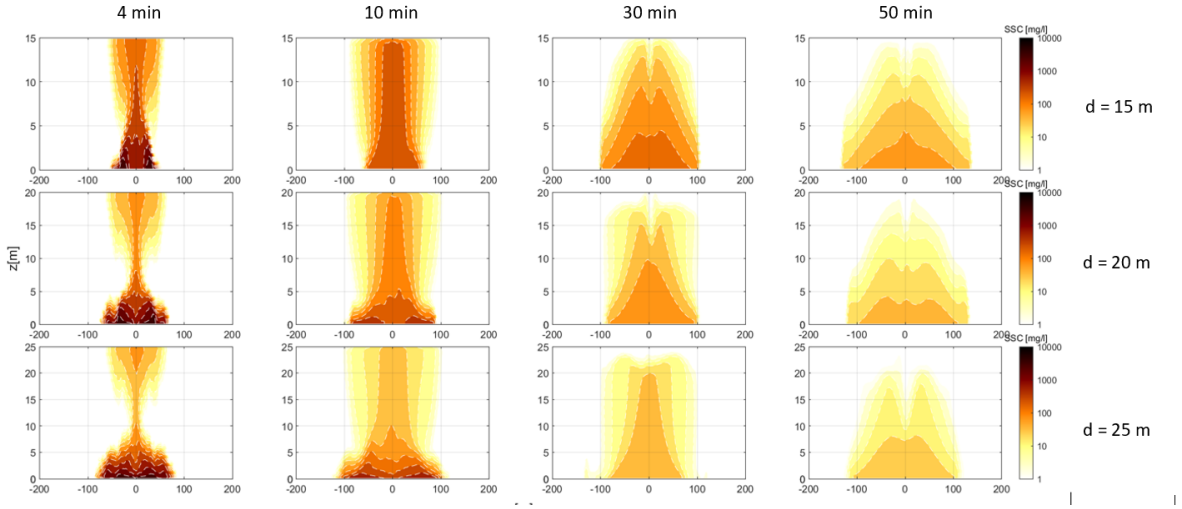

Figure D.1: SSC cross-sections at different plume ages for depths of 15, 20 and 25 [m], respectively. Overflow density $\rho_{overflow} = 1100 kg/m^3$ and Cross-flow velocity $u_{cf} = 0.75 m/s$

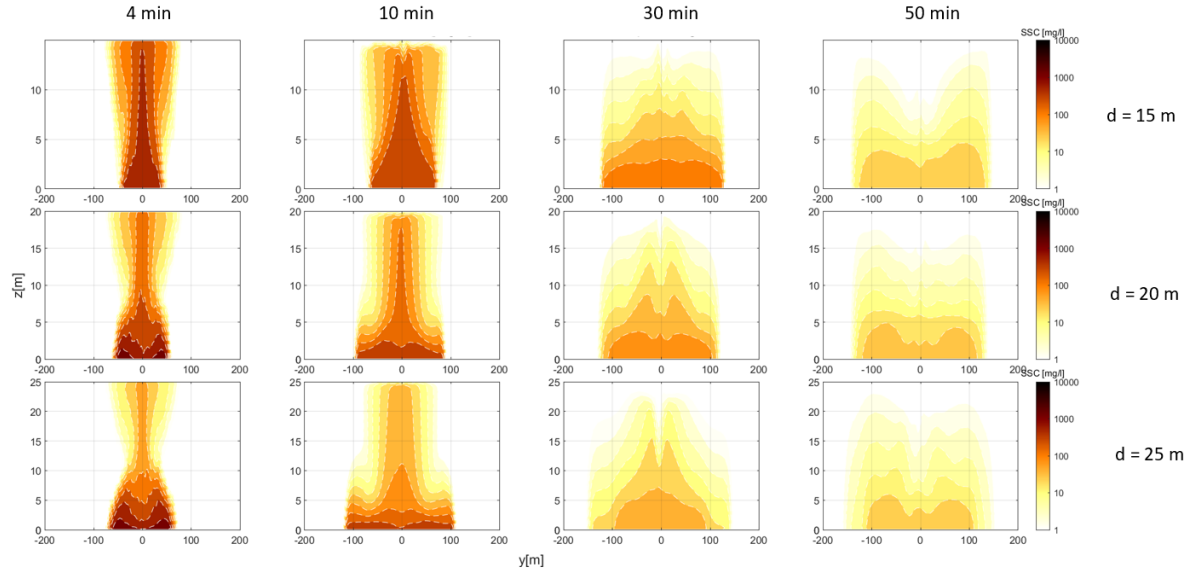

Figure D.2: SSC cross-sections at different plume ages for depths of 15, 20 and 25 [m], respectively. Overflow density $\rho_{overflow} = 1100kg/m^3$ and Cross-flow velocity $u_{cf} = 1.25m/s$

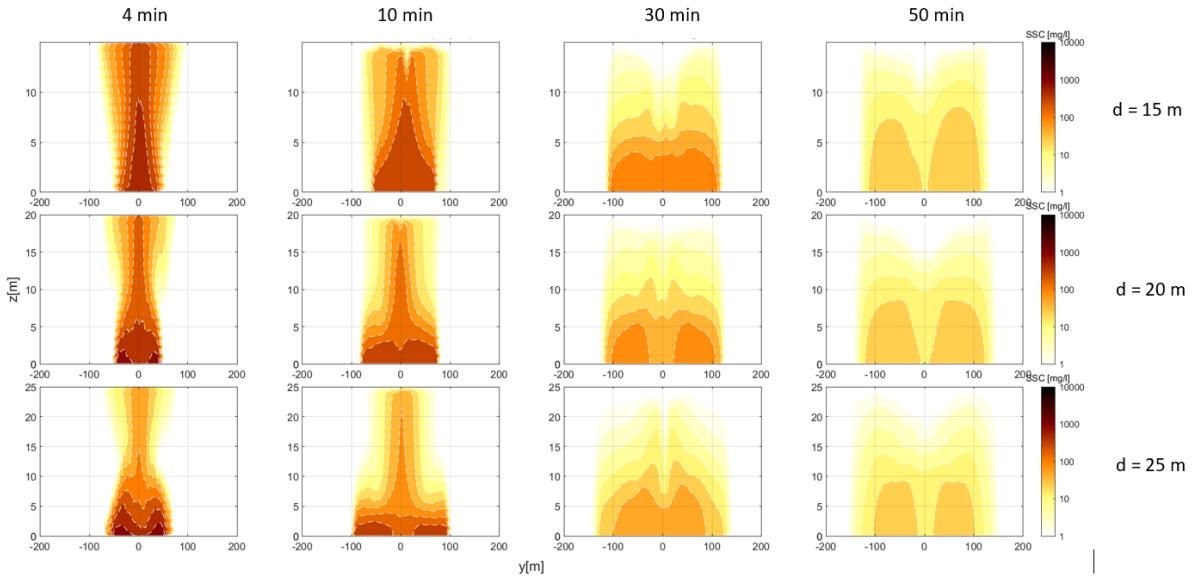

Figure D.3: SSC cross-sections at different plume ages for depths of 15, 20 and 25 [m], respectively. Overflow density $\rho_{overflow} = 1100kg/m^3$ and Cross-flow velocity $u_{cf} = 1.5m/s$

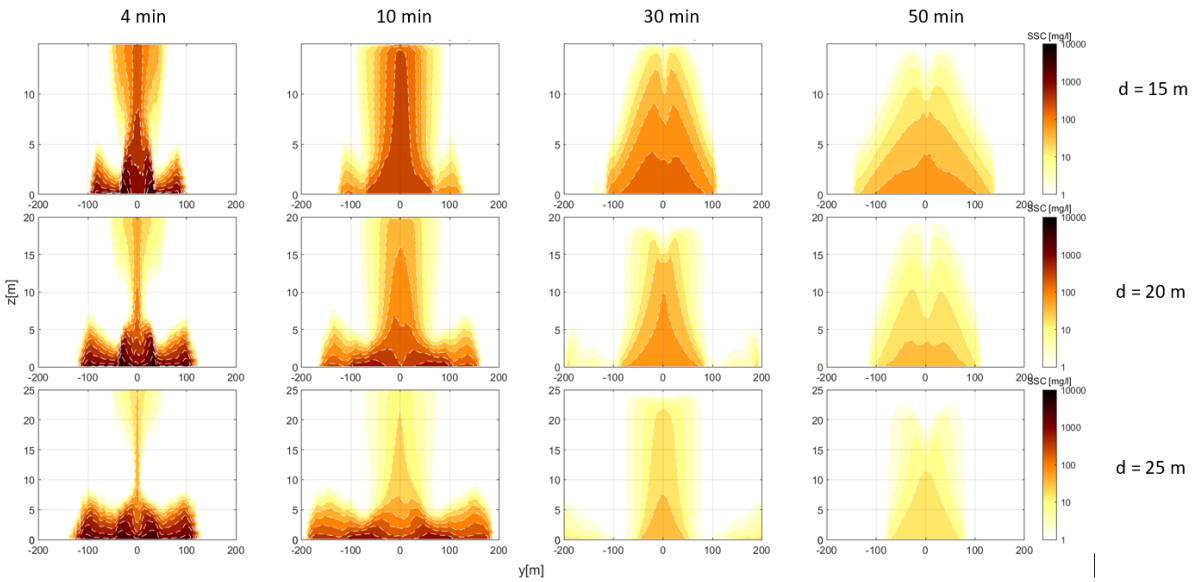

Figure D.4: SSC cross-sections at different plume ages for depths of 15, 20 and 25 [m], respectively. Overflow density $\rho_{overflow} = 1200 kg/m^3$ and Cross-flow velocity $u_{cf} = 0.75 m/s$

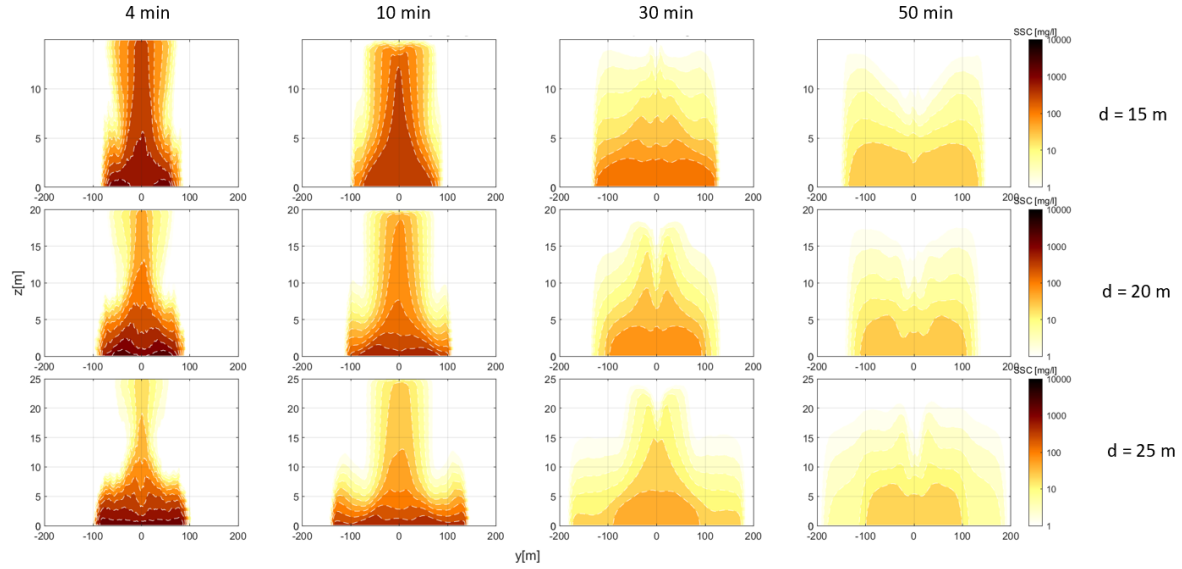

Figure D.5: SSC cross-sections at different plume ages for depths of 15, 20 and 25 [m], respectively. Overflow density $\rho_{overflow} = 1200 kg/m^3$ and Cross-flow velocity $u_{cf} = 1.25 m/s$

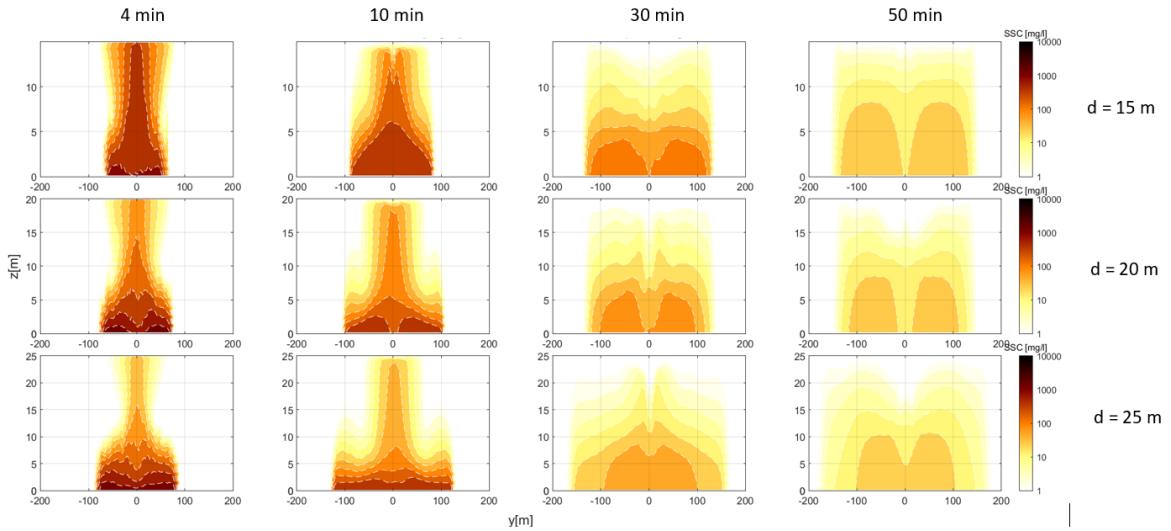

Figure D.6: SSC cross-sections at different plume ages for depths of 15, 20 and 25 [m], respectively. Overflow density $\rho_{overflow} = 1200kg/m^3$ and Cross-flow velocity $u_{cf} = 1.5m/s$